KeAi
CHINESE ROOTS
GLOBAL IMPACT

Available online at www.sciencedirect.com

ScienceDirect

Green Energy & Environment 10 (2025) 1838−1862

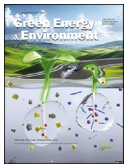

www.keaipublishing.com/gee

Review Article

Heteroatom-functionalized carbon nanoarchitectonics: Unlocking the doping effects for supercapacitor electrode design

Pragati A. Shinde [a,*], Lok Kumar Shrestha [a,b], Katsuhiko Ariga [a,c,*]

[a] Research Center for Materials Nanoarchitectonics (MANA), National Institute for Materials Science (NIMS), 1-1 Namiki, Tsukuba 305-0044, Ibaraki, Japan
[b] Department of Materials Science, Institute of Pure and Applied Sciences, University of Tsukuba, 1-1-1, Tennodai, Tsukuba 305-8573, Ibaraki, Japan
[c] Graduate School of Frontier Sciences, The University of Tokyo, 5-1-5 Kashiwanoha, Kashiwa, Chiba 277-8561, Japan

Received 5 August 2024; revised 29 January 2025; accepted 26 February 2025
Available online 5 March 2025

Abstract

This review focuses on the significant impact of heteroatom doping in enhancing the electronic properties and electrochemical performance of carbon materials for supercapacitors (SCs). Incorporating heteroatoms such as nitrogen, sulfur, phosphorus, fluorine, and boron modifies the carbon structure, creates defects and increases active sites, which improves electronic conductivity, ion accessibility, and surface wettability and reduces ion diffusion barriers. Additionally, certain heteroatoms can participate in electrochemical reactions, further enhancing SC performance. Although research in this area is still emerging, a deeper understanding of the mechanisms behind single and multi-doping systems is essential for developing next-generation materials. Future strategies for improving heteroatom-doped carbon materials include increasing heteroatom content to enhance specific capacitance, selecting suitable heteroatoms to expand the potential window and improve energy density, utilizing advanced in situ characterization techniques, and exploring the use of these materials in cost-effective SCs. The potential of heteroatom-doped carbon materials for SCs is promising, with their ability to improve energy density, power density, and cycling stability, making them competitive with other energy storage technologies. These advancements will be key to broadening their practical applications, including electric vehicles, portable electronics, and grid energy storage, and will contribute to more efficient, long-lasting, and environmentally friendly energy storage solutions.

Keywords: Carbon; Nanoarchitectonics; Supercapacitor; Electrode; Energy storage

1. Introduction

Mankind's abundance depends on available resources and energy. We have used materials and energy sources as they are. In the process, humans have learned that materials can be processed to produce more useful effects. Since materials are limited, it is also important to use them effectively. The energy sources used by humankind have also changed along with technological progress. Fossil fuels have brought about significant advances, but their use is limited. There are strong indications that a shift to other energy sources is needed. Primarily, it is crucial to switch to renewable energy sources [1−5]. Additionally, the growth of fossil fuel-dependent industries has led to significant environmental drawbacks, underscoring the urgency for achieving carbon neutrality [6−8]. The shortage of fossil fuels and the threat of global warming necessitate rapid advancements in energy storage technologies, such as rechargeable batteries and supercapacitors (SCs), to sustain a low-carbon, sustainable economy [9,10]. Rechargeable batteries are indispensable for powering electric vehicles (EVs) and storing renewable energy [11]. However, their performance is often limited by the

* Corresponding authors.
E-mail addresses: SHINDE.PragatiAnkush@nims.go.jp (P.A. Shinde), ARIGA.katsuhiko@nims.go.jp (K. Ariga).
Peer review under the responsibility of Editorial Board of Green Energy & Environment

https://doi.org/10.1016/j.gee.2025.02.007

sluggish diffusion of ions through the bulk of active materials, constraining their power density. On the other hand, SCs, which store energy through surface charge rather than bulk ion diffusion, can deliver high power density, making them well-suited for applications that demand rapid energy delivery. Yet, their reliance on surface charge storage generally results in a lower energy density than batteries, emphasizing the need for ongoing research to enhance their energy storage capabilities.

The progress of material science has accompanied the history of humankind. Never satisfied with materials as they are, humankind has developed science and technology to create materials freely. In particular, the progress of material science since the 20th century has been remarkable. These studies have paved the way for the creation of desired substances. The development of nanotechnology has further accelerated this movement. Nanotechnology has made it conceivable to perceive structures at the atomic and molecular levels [12–14]. It has also made it likely to employ structures at the nanoscale level [15–17]. It has also made analyzing physical properties at the nanoscale level possible [18–20]. Such developments have highlighted the importance of nanostructure control in functional structures. The progress of materials science and the conception of nanotechnology have occurred in parallel. However, it is now time for the two major technologies to merge. This is the formation of materials based on information from nanotechnology [21,22]. Nanoarchitectonics is a perception that occupies a position of post-nanotechnology. As Richard Feynman laid the foundation for nanotechnology in the mid-20th century [22,23], Masakazu Aono projected the concept of nanoarchitectonics at the beginning of the 21st century [24,25]. Nanoarchitectonics is the architecture of practical material systems from nano-units (atoms, molecules, and nanomaterials) [26]. It can be a fusion of nanotechnology and various material sciences.

Methodologies for assembling materials from units in this way have existed in the past science and technology. For example, the formation of supramolecular structures by self-assembly [27–29], the preparation of metal–organic frameworks (MOFs) by complex chemistry [30–33], or the development of covalent organic frameworks (COFs) by polymer chemistry [34–36] are typical examples. These studies can also be considered a portion of nanoarchitectonics. The material synthesis power of nanoarchitectonics has also been deployed in various applications. Various catalysts [37–39], photocatalysts [40–42], sensors [43–45], devices [46–48], nano- and micro-robots [49–51], molecular machine [52–54], environmental remediation [42,55,56], biomass utilization [57–59], drug delivery [60–62], cell control [63,64], and medical fields [65–67] also utilize the concept of nanoarchitectonics. Among their wide range of applications, the use of nanoarchitectonics concepts in energy-related fields is remarkable. Notable applications include fuel cells [68–70], solar cells [71–73], various batteries [74–76], and SCs [77–79]. The nanoarchitectonics methodology fabricates electrode materials with the desired structures and properties. There are also examples of photocatalytic water splitting for hydrogen production [80–82] and energy generation from various sources [83–85]. The socially demanding energy field requires materials with high functional efficiency. The nanoarchitectonics approach can meet this demand.

Examples of applications of the nanoarchitectonics concept in energy-related fields are illustrated below. Bogachuk et al. proposed a sophisticated synthesis of perovskite solar cells using carbon-based back-electrodes under nanoarchitectonics in entirely printed perovskite solar cells [86,87]. Nanocavities were introduced into the mesoporous metal oxide layer using a sacrificial film of polystyrene. Thereby, nonradiative recombination is greatly suppressed. As a result, larger perovskite crystals could be grown within the oxide scaffold. Zhong et al. studied a heterostructured photocatalyst constructed with the strategy of Z-scheme WO_x/Cu-g-C_3N_4 heterojunction nanoarchitectonics [87]. This innovative approach was developed by integrating mechanochemical pre-reactions with thermal condensation processes at high temperatures. Superior thin g-C_3N_4 nanosheets were modified with copper nanoparticles. Additionally, semiconductor nanocomposites were incorporated to enhance the charge carrier separation and transport efficiency within the composite system.

Carbon materials are crucial in SCs electrode research due to their inherent advantages. Initially, pure carbon materials provide EDLC capacitance, but when doped with heteroatoms, they exhibit pseudocapacitive behavior [88]. Despite the high capacitance of porous carbon materials, their conductivity often diminishes with increased porosity and specific surface area, limiting power capacity [89]. To enhance energy and power density, doping carbon materials with heteroatoms (N, O, S, B, P, F) to introduce pseudo-capacitance has gained significant attention [90]. Pseudocapacitive materials are of great interest for energy storage systems due to their ability to deliver high specific capacity and rapid charge/discharge rates, prompting significant research efforts in this area [91,92]. Bahadur et al. presented hybrid nanoarchitectonics of ordered mesoporous C_{60}–BCN approach to bridge the performance gap for SCs and lithium-ion batteries [93]. They developed ordered mesoporous hybrids of fullerenes and boron carbide with a high surface area using the uniquely structured mesoporous silica KIT-6 as a hard template. The hybrids, decorated with C_{60} nanostructures, exhibited ordered mesoporosity and a high surface area and functionalized surfaces that effectively facilitated intermolecular electron transfer enabled by the C_{60}-derived structure.

This review highlights the transformative role of heteroatom doping in enhancing the electrochemical performance of carbon materials for SCs. Incorporating heteroatoms such as nitrogen, sulfur, boron, phosphorus, and fluorine into carbon structures introduces defects, improves electronic conductivity, increases active sites, and enhances surface wettability, ultimately boosting ion accessibility and reducing diffusion barriers. Certain heteroatoms can also participate in electrochemical reactions, further optimizing performance. Future strategies focus on increasing heteroatom content, selecting optimal dopants to expand the potential window, and utilizing advanced characterization techniques. These advancements could broaden the practical applications of SCs in electric

vehicles, portable electronics, and grid energy storage, contributing to more efficient and sustainable energy solutions.

2. Introduction to supercapacitors

Supercapacitors (SCs) have emerged as crucial energy storage systems owing to their exceptional qualities of excellent power density, rapid rates, low maintenance, safety, and excellent stability, which make them perfect for various purposes in transportable electronics, power backups and hybrid vehicles [9,94]. SCs are categorized into two categories, namely, electrochemical double-layer capacitance (EDLC) and pseudocapacitance, with EDLC operating on the Helmholtz double-layer principle and pseudocapacitance involving Faradaic charge transfer [95]. Compared to batteries, SCs charge much faster and maintain a long lifecycle due to negligible volume expansion during charge cycles [11,96]. However, electrode and electrolyte choices primarily influence their energy density. Active materials are pivotal in determining SCs performance, affecting overall effectiveness [97]. This section distinguishes the charge storage mechanism for EDLC, pseudocapacitors, and battery-type energy storage systems.

2.1. Electric double-layer capacitance (EDLC)

The EDLCs are the most widely used and extensively researched type of SCs in which capacitance is generated via the adsorption of anions and cations at the electrode and electrolyte interface [98]. During the charge and discharge processes, the configuration of charges within the Helmholtz double layer generates a displacement current. Due to the materials rapid response to potential changes and their inherent physical reaction characteristics, EDLCs can deliver energy fast. However, due to the restricted area of the electrode surface, the energy storage capacity is limited and significantly lower than that of pseudocapacitors and rechargeable batteries [99]. The EDLC capacitance can be expressed as follows:

$$C_{dl} = \frac{Q}{V} = \frac{\epsilon_r \epsilon_0 A}{d} \tag{1}$$

Where C_{dl} is the capacitance, Q is the charge transferred at potential V, ϵ_r is the dielectric constant of the electrolyte, ϵ_o is the dielectric constant of vacuum, d is the distance of charge separation, and A is the area of the electrode.

When C_{dl} remains constant for EDLCs, the following equation for the response current I can be derived from Equation (1)

$$I = \frac{dQ}{dt} = C_{dl}\frac{dV}{dt} \tag{2}$$

Here, t is the discharge time.

If the applied voltage V changes linearly over time t, in a way that $V=V_0+vt$, V_0 represents the initial voltage, and v is the sweep rate, the relationship can be expressed as

$$I = C_{dl}v \tag{3}$$

As per the above equation, the current is proportional to the sweep rate. Alternatively, when a capacitor is charged or discharged at a constant current, the voltage will increase during charging or decrease during discharging at a steady rate, as given by Equation (3). Consequently, a triangular charge/discharge profile is anticipated, as shown in Fig. 1b and c. Carbon-based materials, including activated carbons (ACs), carbon nanotubes (CNTs), and graphene, are recognized as EDLC SCs [100,101]. Graphene is extensively utilized as an active material in SCs due to its exceptional properties, including a large surface area, excellent electrical conductivity, high thermal and mechanical stability, and flexibility. CNTs are classified into two types based on their synthesis: single-walled (SWCNTs) and multi-walled (MWCNTs) [102]. Using CNTs as electrode materials in energy applications has significantly enhanced performance, especially in achieving high capacitance. Meanwhile, as π-electron-rich carbon precursors, fullerenes can yield high-surface-area carbons with well-controlled morphology and shape. Carbon derived from fullerenes offers outstanding characteristics, including a large surface area and chemical stability [103].

2.2. Pseudocapacitors

Unlike EDLCs, pseudocapacitors store charge through redox processes involving fast and reversible redox reactions on or near the electrode surface. Pseudocapacitive materials exhibit battery-like redox reactions but at comparable rates to capacitors. According to the fundamental theory by Conway, which explains pseudocapacitors working mechanisms, the charge storage in pseudocapacitors involves two different processes: (i) surface redox pseudocapacitance and (ii) intercalation pseudocapacitance.

2.2.1. Surface redox pseudocapacitors

For the surface redox pseudocapacitors, charge storage primarily arises from charge transfer, specifically through redox reactions at the electrode surface. As shown in Fig. 1d–f, the CV and GCD curves for the surface redox pseudocapacitor closely resemble those of carbon-based materials illustrated in Fig. 1a–c. Despite these similarities in profile, pseudocapacitors store charge not only through a double-layer mechanism. Instead, they rely on electric double-layer and surface redox reactions for charge storage [105]. Materials exhibiting these electrochemical characteristics are known as pseudocapacitive materials. Metal oxides are widely used as surface redox pseudocapacitive materials [106]. RuO_2 was the first pseudocapacitive material studied, demonstrating fast electron and ion conductivity features. Other metal oxides, such as MnO_2, WO_3, and Fe_2O_3, also exhibit similar surface redox pseudocapacitance. The multiple valence states of these materials allow rapid and reversible faradaic reactions at the electrode surface, differentiating them from EDLCs [40]. Compared to EDLCs, pseudocapacitors are superior as they store more charge and offer high charge-discharge rates.

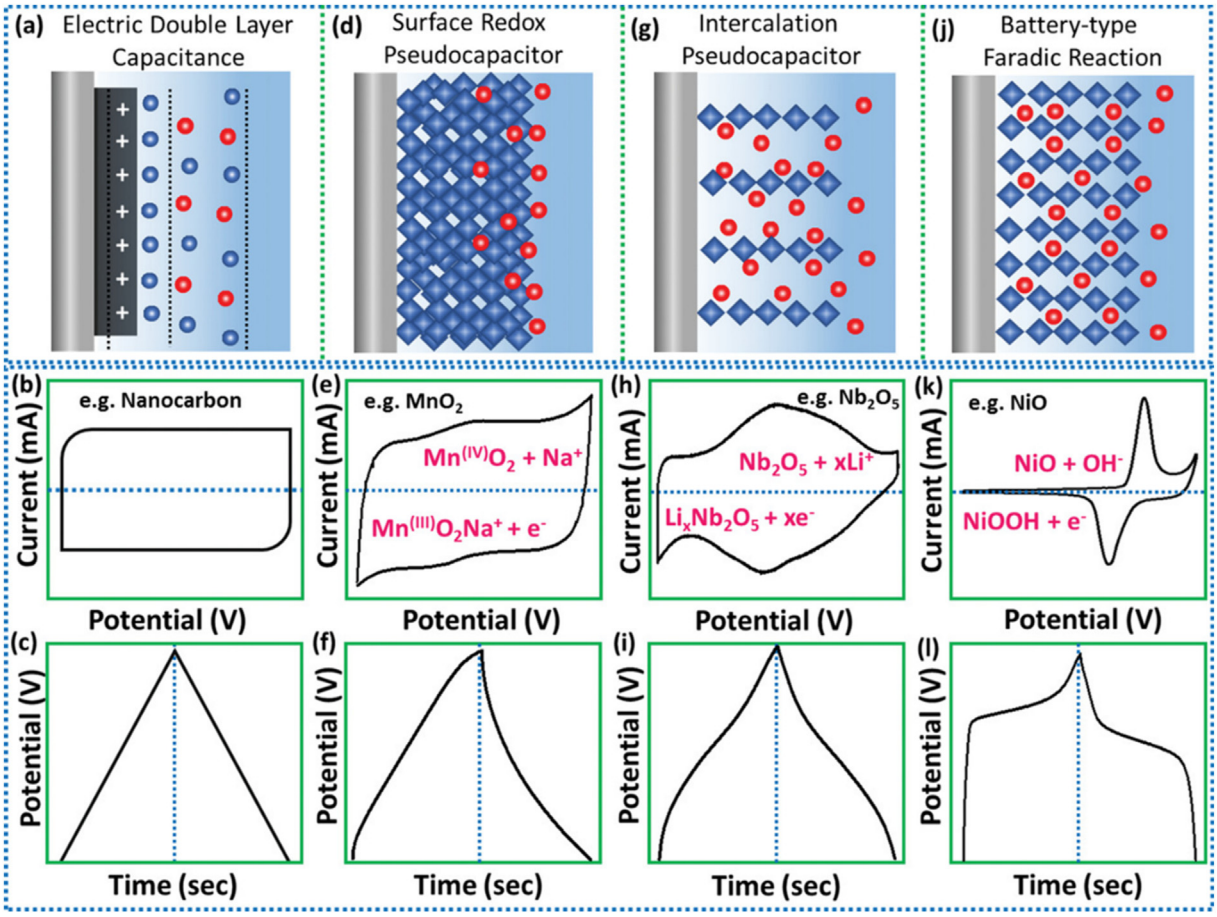

Fig. 1. Illustration depicting different charge storage mechanisms along with their corresponding electrochemical characteristics, including CV and GCD curves: (a–c) electrical double-layer capacitor, (d–f) surface redox pseudocapacitor, and (j–l) faradaic battery type. Reprinted with permission from Ref. [104] Copyright (2020), Wiley-VCH Verlag GmbH & Co. KGaA.

Fig. 1e and f demonstrate redox pseudocapacitors charge storage mechanism and electrochemical features. The charge storage mechanisms in EDLCs and pseudocapacitors differ due to the distinct charge-storing processes and the types of electrode materials employed. However, similarities in their electrochemical characteristics come from the relationship between potential and charge accumulation at the electrode/electrolyte interface or within the internal surface, which results from adsorption/desorption processes. These electrochemical characteristics are essential for differentiating materials and assessing their specific capacitance. Typically, conducting polymers and metal oxides are the main materials used in pseudocapacitors and are known as pseudocapacitive materials [107].

2.2.2. Intercalation pseudocapacitors

The layered materials, for example, MoO_3, Nb_2O_5, MoS_2, WS_2, etc., facilitate faradaic charge transfer reactions by intercalating electrolyte ions into their layers without undergoing phase changes [108]. This rapid and reversible charge storage mechanism is comparable to or surpasses surface redox pseudocapacitors, known as intercalation pseudocapacitance; Dunn and Simon defined this mechanism. Intercalation pseudocapacitors exhibit unique SCs characteristics, such as current being directly proportional to the scan rate, capacitance not varying linearly with charge time, and minimal change in peak voltage with scan rate. A key advantage of these pseudocapacitors is that the materials remain phase-stable throughout the electrochemical process [109]. The charge storage mechanism in intercalation pseudocapacitors extends beyond the surface, engaging the bulk of the active material in a reversible redox process. Fig. 1g–i illustrates the electrochemical properties of intercalation pseudocapacitors, using a typical Nb_2O_5 material as an example.

2.3. Battery-type charge storage

The main difference between battery-type and capacitor-type materials lies in their redox processes. The electrode material undergoes phase changes during electrochemical Faradaic reactions in battery materials [110]. Additionally, the voltage of battery-type materials remains steady during charge–discharge tests by the phase change law and the Nernst equation, as shown in Fig. 2j-l. Therefore, electrodes with diffusion-controlled redox reactions (battery-type) exhibit distinct redox peaks in the cyclic voltammetry (CV) curves

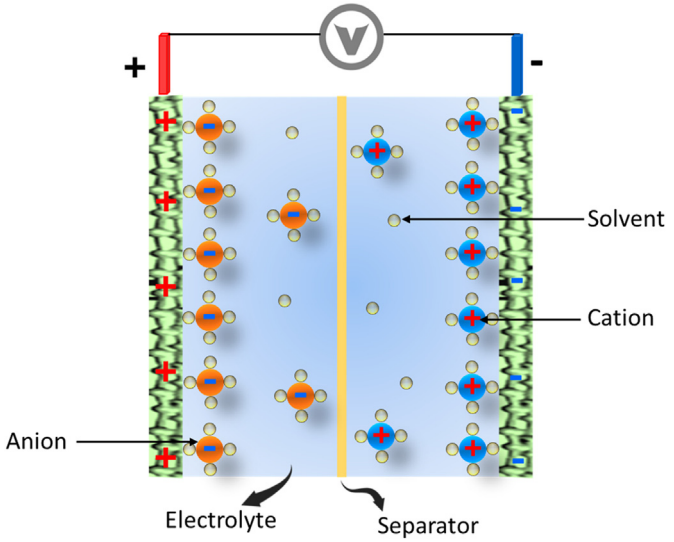

Fig. 2. Schematic presentation of carbon-based SC.

and a plateau in the charge–discharge profile, similar to a battery [111]. Materials based on Ni, Co, and Cu are typical examples of battery-type materials [112]. Unlike capacitors, calculating the specific capacity (mAh g^{-1}) is crucial, as total capacitance does not remain constant across the entire voltage range. The specific mass of the electrode determines the number of electrons and ions intercalated into the active electrode material. Battery-type electrodes offer a higher energy density than EDLCs and pseudocapacitors, making them particularly valuable for applications requiring significant energy output.

3. Research progress on carbon materials for supercapacitors

Over the past decades, substantial progress has been achieved in the fundamental understanding and design of electrode materials for energy storage devices. Carbon-based materials are highly preferred for EDLC SCs because of their excellent electrical conductivity, large surface area, chemical stability, and versatile properties [98,113]. Various forms of carbon materials, like activated carbon, carbon nanotubes (CNTs), graphene, carbon aerogels, and fullerenes, have been thoroughly investigated and utilized to improve the performance of SCs [10,114,115]. Carbon materials are the basis of SC electrodes, typically consisting of an anode and cathode deep in the electrolyte solution, separated by a porous membrane that facilitates electrolyte penetration (Fig. 2). This physical interface enables carbon-based SCs to achieve rapid charge and discharge cycles, delivering significant power output within seconds. Despite these advantages, commercially available carbon-based SCs utilizing activated carbons encounter challenges in organic electrolytes, where their energy densities typically remain < 10 Wh kg^{-1} [116]. These limitations arise from slow mass diffusion and restricted charge accumulation processes within the activated carbon electrodes.

To address this problem, considerable efforts have been directed towards enhancing the energy density ($E = 0.5\ CV^2$) of carbon-based SCs. Maximizing energy density in carbon-based SCs is crucial, focusing on electrode capacitance (C) and electrolyte potential (V). Activated carbon materials with activating agents like $ZnCl_2$ aims to increase surface area. However, this can sometimes lead to issues like hidden pores and broad pore size distributions, which may affect conductivity and performance negatively [117]. Introducing doping defects and functional groups seems promising to enhance electrochemical activity, surface polarization, and electrical conductivity [118]. These defects can modify carbon materials' electronic structure and surface chemistry, which is crucial for enhancing their performance in SCs. Researchers employ CVD, pyrolysis, and specific doping methods during synthesis to precisely control doping levels and introduce particular defects [119,120]. Each heteroatom used for doping introduces unique properties that can significantly influence the features of carbon-based materials [121]. Therefore, it is imperative to carefully optimize the doping strategy according to SCs specific requirements and applications, ensuring enhanced performance and efficiency tailored to different operational conditions and environments [122].

3.1. Single heteroatom functionalized carbon materials for supercapacitors

The development of SC electrode materials has advanced from using porous carbon materials initially focused on providing EDLC capacitance to heteroatom-doped materials demonstrating pseudo-capacitive behavior. While many porous carbon materials can deliver high capacitance, their electrical conductivity often declines as porosity and surface area increase, significantly restricting their power capability. Introducing pseudocapacitance through doping functional groups or heteroatoms (such as N, O, S, B, P, and F) into carbon materials has become a widely adopted strategy to enhance energy and power densities. Compared to EDLC materials and battery materials with EDLC characteristics, pseudo-capacitive materials can achieve both high specific capacity and rapid charge–discharge rates, prompting substantial research into pseudocapacitive materials and associated energy storage systems. Heteroatom-doped materials have been extensively utilized in SCs; however, the heteroatom content alone does not solely determine the materials performance. Incorporating heteroatoms into carbon materials is crucial for modifying their electron-donor characteristics, thereby adjusting the electrical and chemical properties of the surface. This heteroatom introduction reduces charge transfer resistance and enhances wettability, improving capacitive performance.

Heteroatom doping is extensively researched and applied in batteries, SCs, and oxygen reduction reaction (ORR), with each type of dopant offering distinct advantages and challenges [123,124]. These heteroatoms introduce additional active sites and advance the electrochemical features of carbon-based electrodes by enhancing wettability and facilitating

faster electron and ion transport [125]. Accordingly, heteroatom-doped SCs exhibit higher capacitance, energy storage capability, and improved stability, making them more efficient and durable for energy-related applications [126]. The choice of dopant, doping level, and the complexity of the doping process play crucial roles in defining the performance of carbon materials [123]. Optimizing the capacitance of doped nanocarbon materials requires a deep understanding of the electron affinity and electronegativity of the dopant compared to those of carbon.

For instance, nitrogen doping improves electronic conductivity and creates more active sites, enhancing battery performance and SCs surface wettability. However, it does not play a direct role in conversion reactions, which can restrict the storage capacity [127]. Sulfur increases interlayer spacing but can lead to uneven distribution and reduced electrochemical performance. Boron enhances electronic conductance and ion adsorption in SCs but minimizes battery improvement. Phosphorus enlarges interlayer distances and enhances ion mobility, benefiting storage performance and broadening SC electrode working windows. However, it can reduce surface wettability and is challenging to integrate due to its large size. Understanding these diverse doping mechanisms is essential for developing highly efficient materials [128–130]. Fig. 3 shows how different heteroatoms can be incorporated into carbon structures to improve the performance of SCs.

3.1.1. Nitrogen-functionalized carbon materials

In recent years, nitrogen has emerged as a main heteroatom that rallies the competence of carbon-based materials for SCs. The N-doped carbon can be developed via two main methods: post-N doping and in situ [131]. The post-nitrogen doping technique includes treating carbon materials with ammonia, urea, or nitrogen plasma to combine N functional species into the material [132–134]. This method is applied to various porous carbon materials, including activated carbon, carbon nanotubes, templated carbon, fullerene, and graphene. Instead, the in-situ method uses N-rich precursors such as polyaniline, polypyrrole, polyacrylonitrile, melamine analogs, and nitrogen-containing ionic liquids to synthesize nitrogen-functionalized carbon materials directly [92,135]. The N 1s XPS spectrum is one of the essential means for exploring the mechanisms by analyzing the states of nitrogen atoms [136]. Typically, the structures of materials encompass four distinct nitrogen configurations: pyridinic N, pyrrolic N, quaternary N, and N-oxide [137,138]. From these, pyridinic-N and pyrrolic-N are primarily accountable for faradaic behavior to give pseudocapacitance [139]. Additionally, quaternary-N increases the electronic conductivity of materials, which is advantageous for SCs [140]. Additionally, including nitrogen in carbon-based materials can alter the electron distribution. This enhancement in the interaction between active electrode materials and electrolytes leads to a substantial increase in the active surface area available for electrolyte ions.

Furthermore, boosting ion transport is crucial for advancing high-performance carbon materials. Hierarchical porous structures play a significant role in this process by offering smooth pathways for ion diffusion, enhancing the rate capability. Additionally, incorporating heteroatoms into the carbon framework offers additional ion storage sites. Utilizing this, Zheng et al. [141] employ N-doped porous carbon from cultivated waste as electrodes for SCs. This study used $ZnCl_2$ to create hierarchical pores and ammonium chloride to introduce nitrogen into ginger-straw-based carbon. The resultant carbon exhibited superior SCs properties, a high surface area of 1186 $m^2\ g^{-1}$, and 5.58% nitrogen. When used for Li-ion capacitors, the device achieved an energy density of 214.6 W h kg^{-1} at a power density of 373.5 W kg^{-1} and 82.7% stability over 10,000 cycles. Chen et al. [142] developed hydrothermal carbonization (HTC) method to create carbonaceous nanofibers (CNFs) and large-scale monolithic hydrogels/aerogels. Using CNFs as templates, they produced N-CNFs with graphitic frameworks by coating CNFs with pyrrole (Ppy), polymerizing, and then carbonizing under N_2 flow at temperatures of 500–1100 °C (Fig. 4a). The nitrogen species and pore structures of CNFs depend significantly on carbonization temperature. With the temperature rise, the diameter of N-CNFs decreased slightly, and N-CNFs-900 showed many interstitial pores (Fig. 4b and c). XPS analysis revealed nitrogen content percentages of 12.14%, 12.04%, 9.57%, 7.22%, and 4.02% for CNFs@Ppy, N-CNFs-500, N-CNFs-700, N-CNFs-900, and N-CNFs-1100, respectively (Fig. 4d). This approach successfully incorporated surface

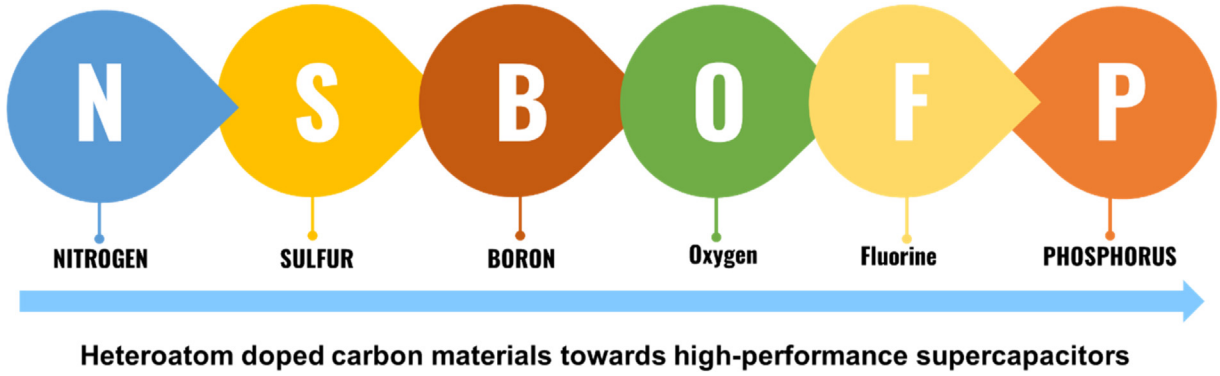

Fig. 3. Schematic representation of the different heteroatoms that can be doped into carbon to enhance SCs performance.

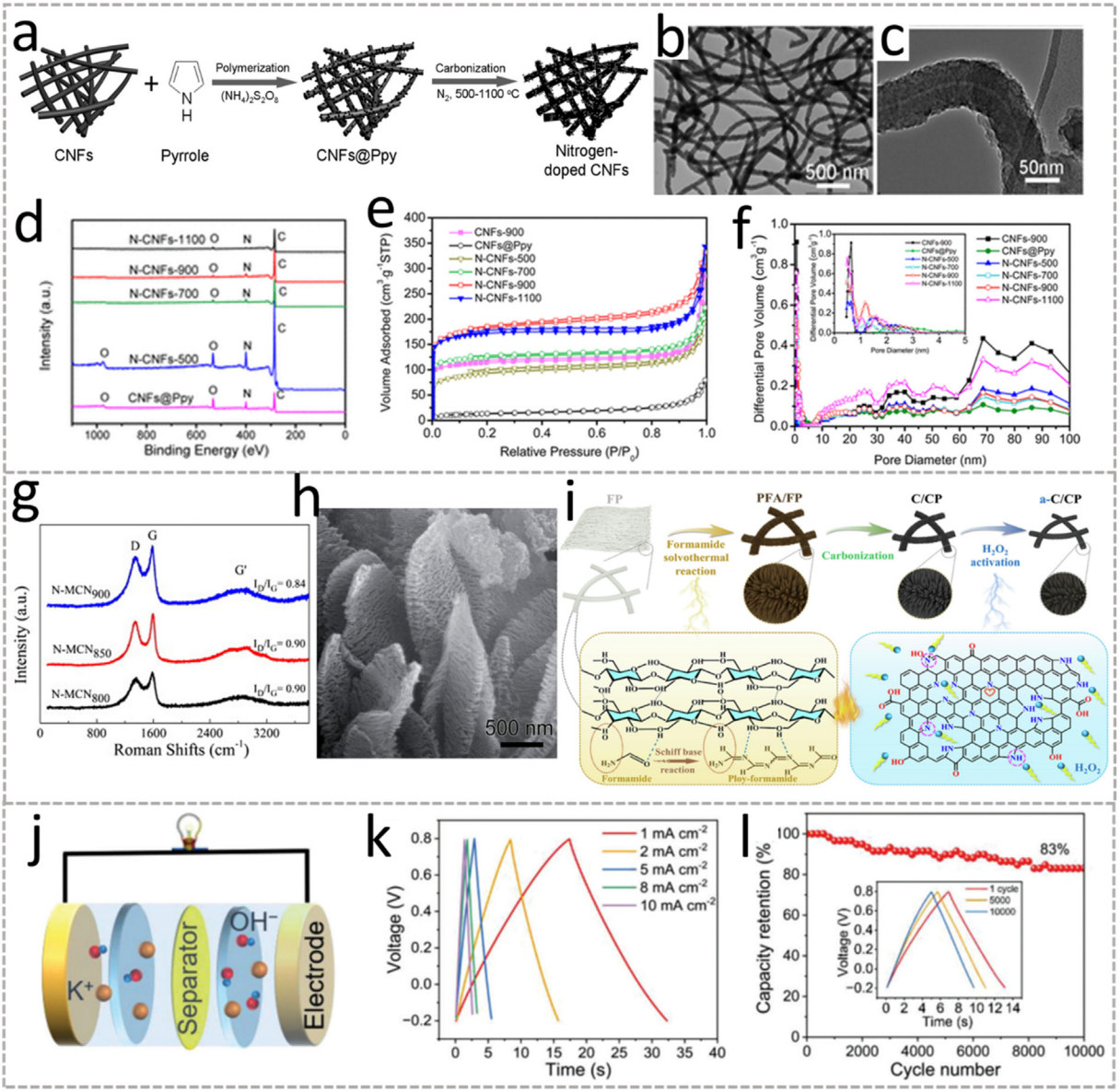

Fig. 4. (a) Synthesis protocol for N-doped CNFs. (b, c) TEM of N-CNFs-900, (d) XPS survey of CNFs@Ppy and N-CNFs. (e) N_2 adsorption–desorption isotherms and (f) pore size distribution (inset: magnified 0–5 nm region) of CNFs-900, CNFs@Ppy, N-CNFs-500, N-CNFs-700, N-CNFs-900, and N-CNFs-1100. Reprinted with permission from Ref. [142]. Copyright (2012) American Chemical Society. (g) The Raman spectra of the N-MCNs. Reprinted with permission from Ref. [143]. Copyright (2015) Elsevier. (h) SEM image of Nitrogen-doped micro/mesoporous carbon net. Reprinted with permission from Ref. [145] Copyright (2016) The Royal Society of Chemistry. (i) Synthesis protocol and mechanism for a-C/CP. Reprinted with permission from Ref. [146]. Copyright (2023) Elsevier. (j) Schematics of SCs device based on N-doped carbon nanotubes, (k) GCD of SCs, and (l) stability measurement of SCs device. Reprinted with permission from Ref. [147]. Copyright (2024) Wiley-VCH Verlag GmbH & Co. KGaA.

functionalities into carbon materials, where nitrogen-containing species created active sites that improved the power density of SCs. The N-CNFs displayed type IV N_2 adsorption–desorption isotherms, signifying the occurrence of micropores and mesopores. The specific surface area increased from 293.63 to 562.51 $m^2\ g^{-1}$ as the temperature increased from 500 °C to 900 °C before slightly decreasing at 1100 °C (Fig. 4 e, f). Electrochemical studies showed that N-CNFs-900 had a capacitance of 202.0 F g^{-1} at 1.0 A g^{-1} and a small equivalent series resistance. Thus, N-CNFs show great potential as electrode materials for SCs. Zhao and coworkers [143] synthesized N-functionalized microporous carbon nanoparticles (N-MCNs) via a polymerization using terephthalaldehyde and *m*-phenylenediamine in dioxane, with 3 mol L^{-1} acetic acid as the catalyst. The resulting polymer was carbonized at different temperatures under the N_2 atmosphere for 4 h. The Raman spectrum (Fig. 4g) exhibited two peaks at 1350 cm^{-1} (D band) and 1580 cm^{-1} (G band). The SCs characteristics were tested in a 6 mol L^{-1} KOH electrolyte. Among the N-MCNs, N-MCN850 displayed the highest capacitance of 254 F g^{-1} at 1 A g^{-1}. Wang et al. [144] prepared N-doped cellulose-derived porous carbon fibers (N–CHPCs) by a bio-template method

with cotton cellulose and urea. When used in large mass-loading (12.8 mg cm^{-2}; 245 μm) aqueous SCs, the N–CHPCs demonstrated outstanding electrochemical performance with a specific capacitance of 295.8 F g^{-1} at 0.1 A g^{-1} and excellent durability. Micro/mesoporous carbon nets with N-doping were effectively developed using block copolymer P123 and dicyandiamide and TiO_2. These carbon nets feature a substantial surface area of around 2144 m^2 g^{-1} and a good N amount of roughly 8.25 wt%. The resultant material showed a highly interconnected structure of disordered nanofibers, as seen in the SEM image (Fig. 4h) [145].

In a recent study by Yan and coworkers [146], SCs performance was investigated using cellulose-derived carbon that was enhanced by two methods: coating with nitrogen-doped carbon nanowire arrays and modifying the pore structure (as shown in Fig. 4i). These electrodes offer several benefits, such as being self-supporting and highly compatible with electrolytes. They feature interconnected conductive fiber networks and a robust porous structure with stable heteroatom-doped carbon coatings. In SC performance tests, they achieved a specific capacitance of 275.6 F g^{-1} at a current density of 0.5 A g^{-1}. Furthermore, the symmetric SCs reached an energy density of 17.5 Wh kg^{-1} and a power density of 12.3 kW kg^{-1}. The three-dimensional networks of nitrogen-doped carbon nanotubes (N-CNT@CF) were fabricated using electrospinning and CVD methods. The incorporation of CNTs and nitrogen-doped CNTs into the carbon fiber networks, along with increased nitrogen content in N-CNT@CF, enhances electronic conductivity and shortens the diffusion path for electrolyte ions [148]. Wang and coworkers have recently developed N-doped activated carbon from bean pulp (BPC) using a one-step process that combines carbonization and CO_2 activation at 1073 K [149]. An environment rich in CO_2 promotes the transformation of nitrogen-containing functional groups. CO_2 can interact with primary amines (R═NH_2), secondary amines (2R═NH), and tertiary amines (3R═N), leading to the formation of amino acid-derived nitrogen (amide-N), which subsequently converts into pyrrolic-N and pyridinic-N.

Chen et al. [150] produced porous nitrogen-doped carbons from bamboo shoots. Bamboo, known for its rapid growth and abundance, is rich in nitrogen-containing compounds like proteins and amino acids, making it suitable for N-doped carbon production. Hydrothermal processing combined with carbonization in an inert environment yielded porous nitrogen-doped carbon materials without templates or additional chemical activation. The material exhibited a substantial BET surface area of up to 972 m^2 g^{-1}, a hierarchically interconnected porous architecture, and a consistent nitrogen content of 3.0 at%. When employed as an electrode in supercapacitors using a KOH electrolyte, this material demonstrated a high capacitance of 412 F g^{-1} and exceptional cycling stability. Li et al. [5] reported N-doped activated carbon (N-AC) from corncob agricultural waste. This material demonstrated a remarkable specific surface area of up to 2859 m^2 g^{-1}, a tightly controlled pore size distribution, and a nitrogen content reaching 4 wt%. When tested in hybrid SCs, the N-AC delivered an impressive energy density of 230 Wh kg^{-1} at a power density of 1747 W kg^{-1}. The enhanced capacitance was ascribed to the faradaic reactions involving N-functionalized species and improved wettability of the pore surfaces. Zhang and coworkers [147] reported flash Joule heating (FJH) technology to synthesize N-doped carbon nanotubes (N-CNTs). FJH technology offers significant advantages in synthesizing and modifying carbon materials owing to its extremely short reaction times and low energy ingesting. This technique does not require a catalyst or particular gas and can be completed in a vacuum system within 1 s. By adjusting the thickness of the PANI and the discharge voltage during the Joule heating procedure, the content of different nitrogen forms can be modified. Authors developed N-CNTs from polyaniline-coated CNT. The symmetric SCs assembled with N-CNTs are illustrated in Fig. 4j. Fig. 4k shows the GCD curves of the device from 1 to 10 mA cm^{-2}. The durability performance was tested for 10000 cycles, where 83% capacitance was retained (Fig. 4l).

Thus, the literature reports indicate that incorporating nitrogen into the carbon matrix significantly enhances the electrical conductivity, surface wettability, and pseudocapacitive properties of the active material, resulting in improved energy storage performance. This integration creates a synergistic effect by combining the structural advantages of carbon with the electrochemical benefits of nitrogen functionalities, positioning these materials as promising candidates for advanced energy storage technologies.

3.1.2. Sulfur-doped carbon for supercapacitors

Due to its attractive properties, sulfur is gaining attention as a heteroatom in energy storage device research [151]. The nearly identical electronegativities of sulfur ($\chi = 2.58$) and carbon ($\chi = 2.55$) result in a covalent bond between sulfur and carbon that is essentially non-polar when doping occurs [152]. However, because the bond lengths of C–S differ from those of C–C, sulfur doping favors the creation of thiophene with carbon [153]. Additionally, sulfur doping can sometimes induce curvature in the otherwise flat graphene sp^2 structure, leading to some distortion in the aromatic system. Sulfur doping in carbon materials presents more challenges than nitrogen doping due to sulfur's larger atomic size and similar electronegativity to carbon. Despite these challenges, recent advancements have highlighted sulfur-doped carbon materials as highly promising for SCs. Incorporating sulfur atoms into the carbon framework enhances the material's conductivity and introduces additional active sites for charge storage. This modification can significantly improve the specific capacitance and energy density of SCs. Moreover, sulfur-doped carbon materials demonstrate outstanding stability, making them well-suited for long-term applications [154]. Yang and coworkers [155] developed S-doped hollow carbon spheres (SHCS) for potassium ion hybrid capacitors. Fig. 5a illustrates the preparation process. The TEM picture shows that SHCS are porous hollow carbon spheres with an outer thickness of ~41 nm (Fig. 5a). The high proportion of C–S–C and C–SO_x–C in the S 2p XPS spectrum specifies that S was

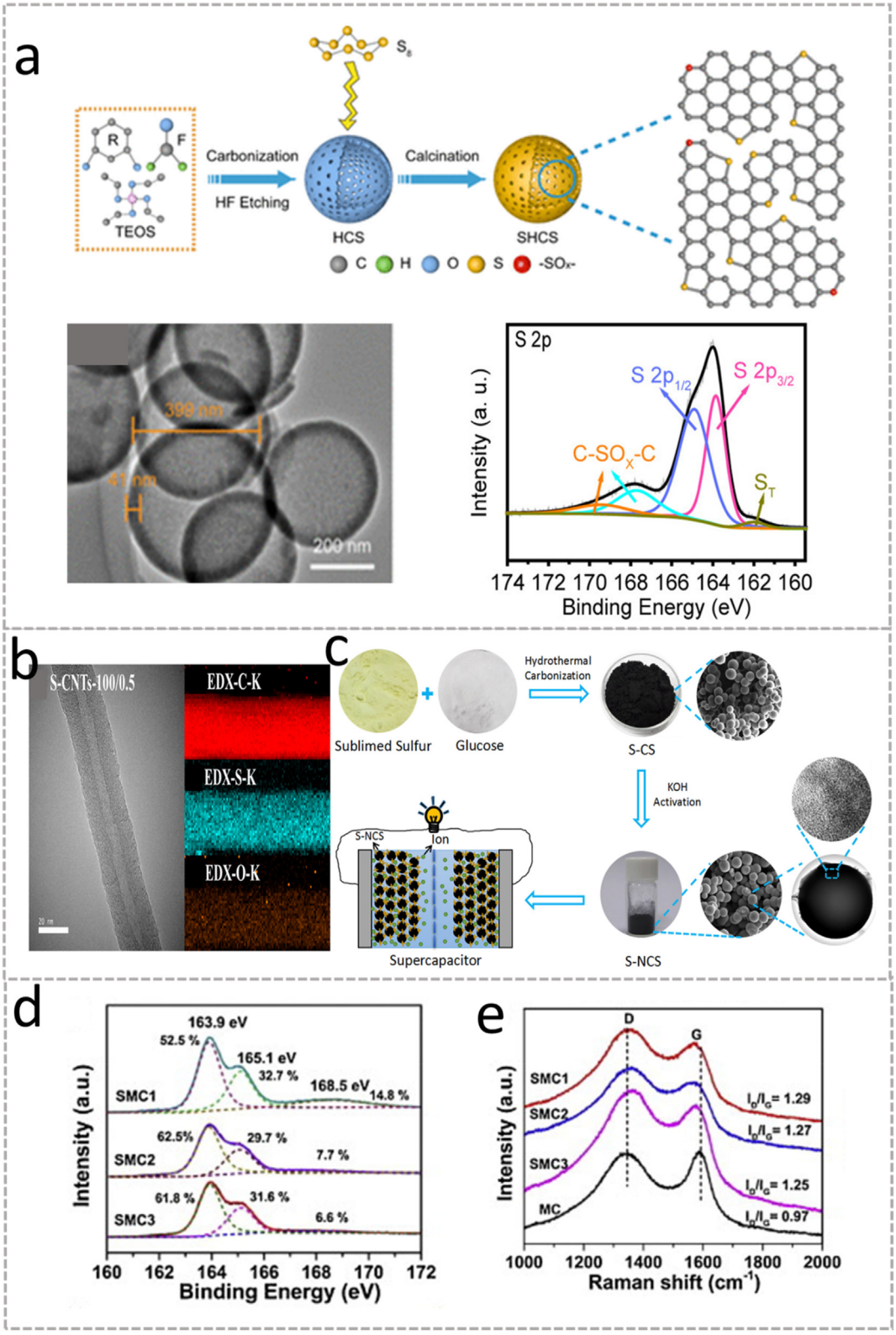

Fig. 5. (a) Schematics protocol for the development of sulfur-doped hollow carbon spheres (SHCS), TEM image, and XPS spectra of S 2p of SHCS. Reprinted with permission from Ref. [155]. Copyright (2021) American Chemical Society. (b) HR-TEM and EDX of S-CNTs. Reprinted with permission from Ref. [156]. Copyright (2021) Elsevier. (c) Schematic protocol for S-doped nanoporous carbon spheres (S-NCS) Reprinted with permission from Ref. [157]. Copyright (2017) Elsevier. (d) XPS and (e) Raman spectra of S-doped mesoporous carbon fibers. Reprinted with permission from Ref. [158]. Copyright (2014) Elsevier.

covalently bonded to the carbon (Fig. 5a). The potassium ion hybrid capacitors cell attained an energy density of 135.6 W h kg^{-1} at 17.7 kW kg^{-1} with good cycling performance.

Kim and coworkers [156] developed sulfur-doped CNTs through the chemical vapor deposition (CVD) technique and investigated the effect of doping on SCs performance. Dimethyl disulfide was utilized as the sulfur-containing carbon source. The STEM-EDX mapping of the S-CNTs synthesized at 1000 °C showed diameters ranging from 28 to 30 nm and CNT wall thicknesses between 8 and 10 nm. The images also confirmed an even spreading of carbon, sulfur, and oxygen throughout the S-CNT surface (Fig. 5b). The electrochemical performance significantly improved after sulfur doping. Another study by Liu et al. [157] developed sulfur-doped nanoporous carbon spheres (S-NCS) containing 0.6% sulfur. The synthesis was achieved through a high-temperature hydrothermal carbonization process utilizing sublimed sulfur and a glucose solution, followed by potassium hydroxide (KOH) activation (Fig. 5c). The S-NCS demonstrated impressive performance with excellent specific capacitance and stability. Sulfur-doped mesoporous carbon fibers, containing 14.0 at% sulfur (29.4 wt.%), were synthesized from $MgSO_4$-infused porous whiskers as templates and sucrose as the carbon precursor. The ideal conditions for synthesis were determined to be a calcination temperature of 600 °C, whisker templates with a smaller diameter, and a carbon-to-template ratio of 1:5. X-ray photoelectron spectroscopy analysis indicated that sulfur predominantly formed thiophene-S (C–S–C) bonds (Fig. 5d). Raman spectra indicated increased defects with higher S content (Fig. 5e). When used as SC electrodes, these fibers significantly increased specific capacitance with rising S content, achieving 221 F g^{-1} at 10 mV s^{-1} and retaining 95% stability. The research highlights that sulfur-doped carbons with higher sulfur concentrations exhibit significant potential as electrode materials for SCs.

In another study by Deng et al. [159] sulfur-doped porous carbon nanosheets (S–PCNS) were created via the direct carbonization and concurrent chemical activation of a cobalt ion-impregnated sulfonic acid ion exchange resin. These S–PCNS exhibit a three-dimensional interconnected network, elevated graphitization levels, notable sulfur content, an extensive specific surface area, and substantial mesoporosity. SEM images reveal micrometer-sized graphene-like nanosheets forming 3D networks. HRTEM images demonstrated a *d*-spacing of 0.33 nm, matching graphite's (002) lattice spacing. Cyclic voltammograms of S–PCNS maintain a rectangular outline up to 1000 mV s^{-1}, representing capacitive properties with fast charging and discharging. The GCD curves reflect high charge–discharge efficiency. The S–PCNS displayed a specific capacitance of 312 F g^{-1} at 0.5 A g^{-1}. The Nyquist plot displays a short Warburg-type line, indicating easy ion diffusion in the S–PCNS, and the low-frequency impedance spectrum is nearly vertical, suggesting almost ideal capacitor behavior. Xue and colleagues [160] reported that exceptional SC performance could be achieved through the redox mechanism, which involves converting a thiocarboxylic acid ester to a sulfone using an external current. This transformation enables the sulfur-functionalized graphene aerogel to achieve a maximum specific capacitance of 1089 F g^{-1} at a current density of 1 A g^{-1} while retaining a notable capacitance of 833 F g^{-1} even at 50 A g^{-1}. Additionally, the material demonstrates a high energy density of 43 W h kg^{-1} at a power density of 38 kW kg^{-1}, indicating its capability to effectively provide both high power and high energy density.

Even though sulfur-doped carbon materials perform a crucial role in enhancing the performance of SCs, maintaining structural stability during synthesis and operation is difficult due to sulfur volatility. Uniform sulfur incorporation is complex, and doped materials often face difficulties in terms of conductivity and durability. Additionally, cost-effective and scalable synthesis methods remain a challenge for widespread applications.

3.1.3. Boron-doped carbon for supercapacitors

Unlike nitrogen and sulfur, boron doping in carbon materials remains less common, presenting a unique opportunity for exploration in carbon research. Introducing heteroatoms can induce defects in nearby sites due to uneven charge distribution. For instance, substituting boron into a hexagonal sp^2-bonded carbon framework results in p-type behavior. This substitution increases the density of hole charge carriers, which modifies the band gap and enhances the material's electronic properties and conductivity [161]. Boron doping can be achieved through various methods, including boron oxide (B_2O_3), arc discharge, laser ablation, hydrothermal synthesis, and CVD, etc. [162] B-doped graphene is generally produced by introducing boron through gas-phase sources, such as H_3BO_3 or BCl_3, or by using autoclave treatments in an inert atmosphere [163]. However, due to the low reactivity of inorganic boron compounds and the high toxicity of organic boron compounds, doping efficiency remains low, making direct boron doping of carbon materials a significant challenge. Additionally, boron-doped materials often contain oxygen elements due to limitations in precursor selection and the surrounding environment [164]. Boron and nitrogen differ by just one electron, and borons atomic size is similar to carbons. When carbon is doped with boron, its structure remains unchanged, making it an excellent candidate for doping carbon materials [165]. By substituting carbon atoms with boron, which has three valence electrons, boron acts as an electron acceptor in the carbon lattice. This substitution shifts the Fermi level into the conduction band, altering the electronic properties of the doped carbon.

Du and coworkers [166] synthesized B-doped carbon (B-HPC) using a one-step calcination process with glucose as the carbon source, boric acid to introduce boron, NaCl as a template, and $ZnCl_2$ as an activation agent were employed (Fig. 6a). The introduction of B surges the surface area from 446.62 to 781.21 m^2 g^{-1}. When B-HPC is employed for SCs, it exhibits a specific capacitance of 379.9 F g^{-1} at 1 A g^{-1}. Umezawa and coworkers [169] prepared B-doped porous carbon by directly carbonizing a boron-based covalent organic

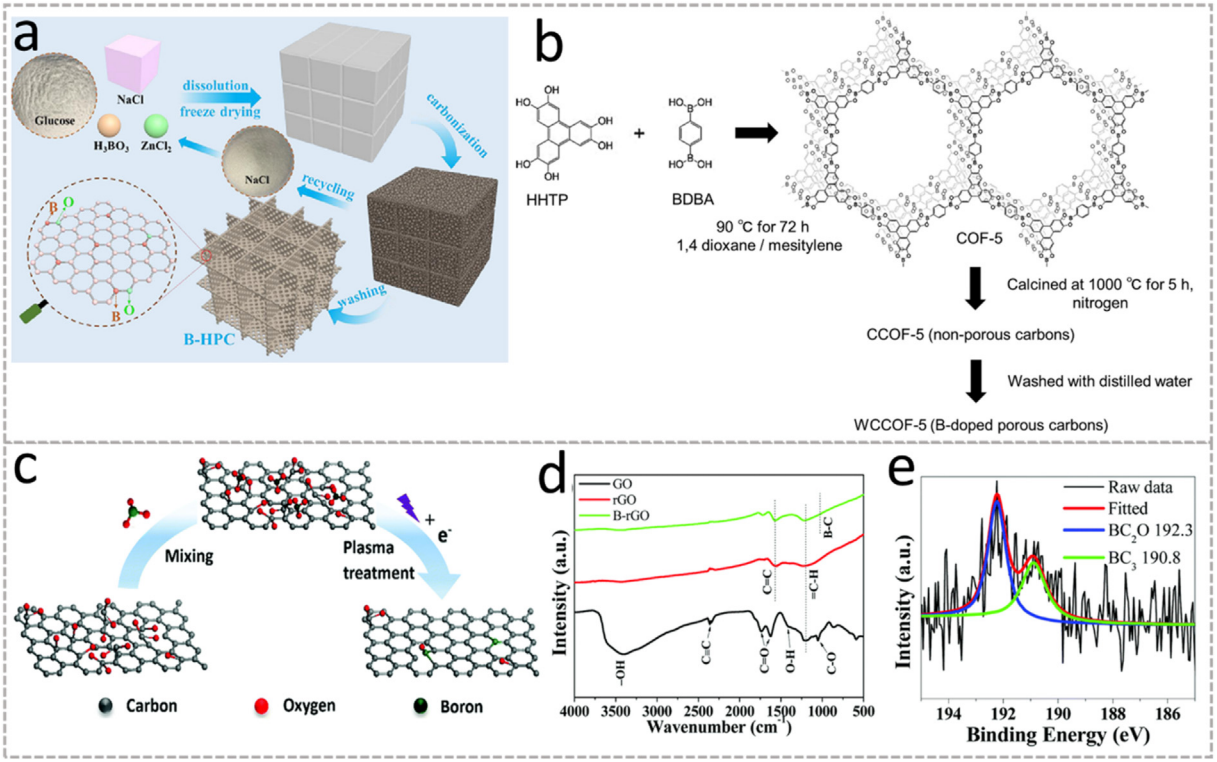

Fig. 6. (a) Synthesis procedure for boron-doped carbon material (B-HPC), reprinted with permission from Ref. [166]. Copyright (2021) Elsevier. (b) COF-5 derived boron-doped carbon, reprinted with permission from Ref. [167]. Copyright (2013) American Chemical Society. (c) B-rGO synthesis protocol using DBD plasma technology. (d) The FT-IR and (e) XPS spectra of B-rGO. Reprinted with permission from Ref. [168]. Copyright (2016) The Royal Society of Chemistry.

framework (COF-5). Fig. 6b demonstrates the synthesis protocol of porous carbon from COF-5. The resulting B-doped porous carbon showed a high charge density of 15.3 μF cm^{-2} when tested for SCs. Han and coworkers [167] reported a solution-based approach to synthesize boron-doped graphene. In this method, graphene oxide (GO) reacts with a borane-tetrahydrofuran adduct, which serves as both a reducing agent and dopant. After drying under mild vacuum conditions, approximately 1 atom percent of boron could successfully be incorporated into the graphene platelets. This process represents the first solution-based technique for producing boron-doped graphene nanoplatelets for supercapacitor applications. In a two-electrode system, the resulting boron-reduced graphene oxide exhibited a high specific capacitance of 200 F g^{-1} at a current density of 0.1 A g^{-1} in an aqueous electrolyte. Li and coworkers [168] prepared B-rGO using DBD plasma technology at ambient conditions. Fig. 6c shows the synthesis procedure. The FT-IR and XPS spectra were employed to study the chemical composition of and surface chemistry of the B-rGO (Fig. 6d and e). The analysis revealed a boron concentration of 1.4 at%, resulting in an impressive capacitance of 446.24 F g^{-1} at 0.5 A g^{-1}, significantly surpassing the performance of undoped graphene. In a recent report by Kim and coworkers [170], B-doped graphene nanoplatelets were synthesized by annealing GO nanoplatelets with B_2O_3. The boron doping level and GO reduction were controlled by varying the annealing temperature. The high boron concentration of 6.04 ± 1.44 atom% was obtained at 1000 °C. These B-doped nanoplatelets unveiled a specific capacitance of 448 F g^{-1}, three times greater than that of pristine graphene nanoplatelets (135 F g^{-1}).

Lu and coworkers [171] reported synthesizing boron-doped carbon spheres using aerosol-assisted spraying (Fig. 7a). HAADF-STEM and EDS mapping reveal the coexistence of C, O, and B elements in the spheres (Fig. 7b). DFT calculations show that B doping creates uneven electrostatic potentials, enhancing the attraction of negative ions compared to pure carbon (Fig. 7c). OH− adsorption energy is significantly higher on B-doped carbon (−277.8 kJ mol^{-1}) than on pure carbon (−113.7 kJ mol^{-1}), with additional atoms like O further increasing this effect (Fig. 7d). B doping enhances K^+ adsorption through stronger Van der Waals and electrostatic interactions, improving overall capacitance (Fig. 7e). Figueiredo and coworkers [172] studied B-doping on SCs performance of ordered mesoporous carbons. The SCs measurements were carried out in 1 mol L^{-1} H_2SO_4, and a high performance was achieved for the electrode with 1.8 wt% boron.

B-doped three-dimensional (3D) cubic ordered mesoporous carbon (B-OMC) was synthesized through a straightforward bubbler-assisted chemical vapor deposition (CVD) technique, using acetylene and triisopropyl borate on Fe-KIT-6 at 700 °C. The produced B-OMC was tested for supercapacitor (SC) applications and showed a significant specific capacitance of 329 F g^{-1}. Additionally, a symmetric SC device assembled with a 1 mol L^{-1} Na_2SO_4 electrolyte achieved an impressive energy density of 10.27 Wh kg^{-1} and a power density of 300.59 W kg^{-1} [173]. B-doped diamonds are commonly used as electrode materials in SCs due to their high ion-accessible surface area,

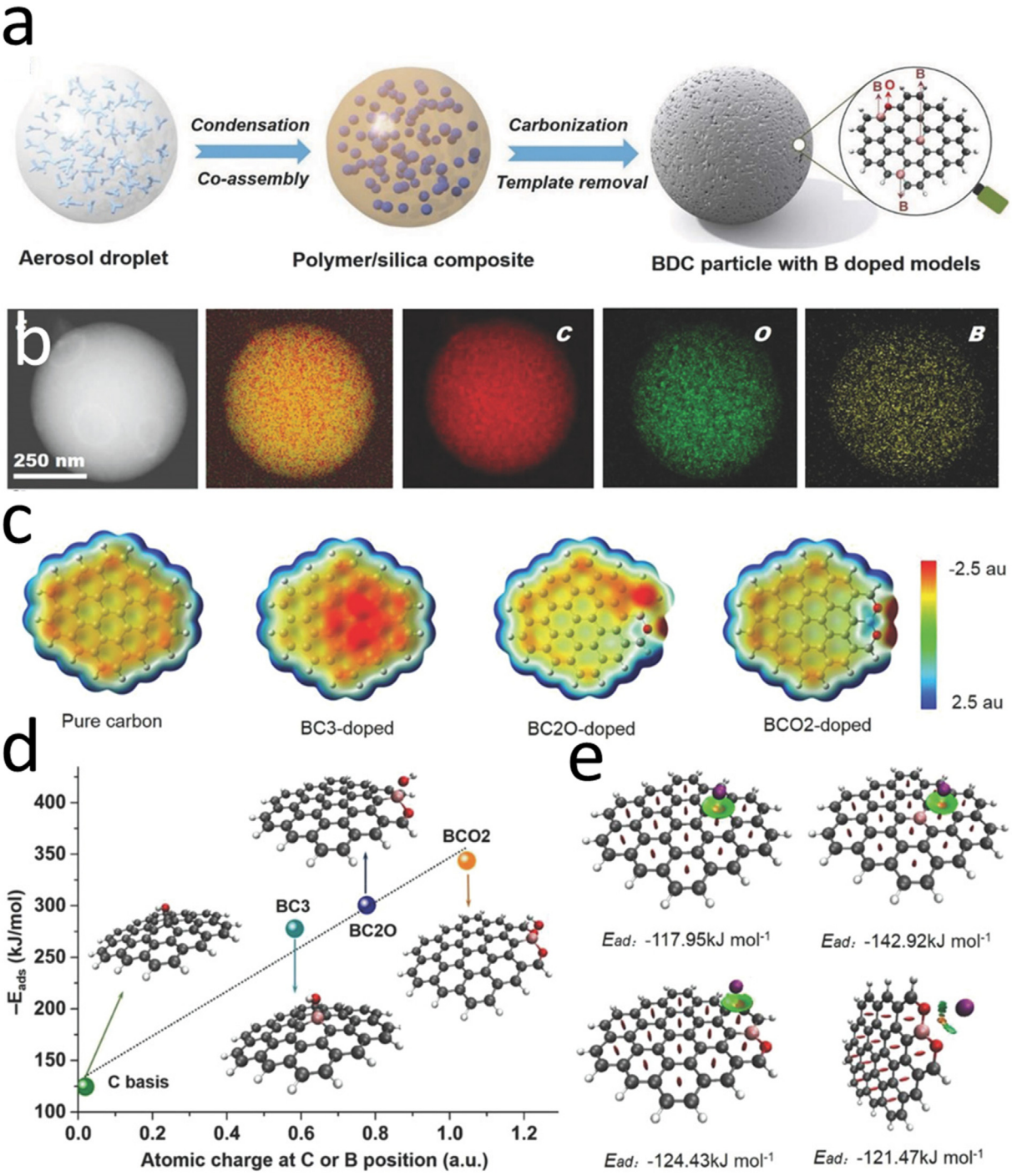

Fig. 7. (a) Preparation of boron-doped carbon spheres (BDC). (b) HAADF-STEM imaging and EDS mapping of a BDC sphere. (c) Electrostatic potential maps for various surface models. (d) Configurations of OH^- adsorption on different carbon surface models, including adsorption energy and atomic charges for carbon and boron. (e) Configurations of K^+ adsorption on carbon surfaces, with energy data presented (Violet: K^+; Cyan: B; Red: O; Black: C; White: H). The sign ($\lambda 2$) ρ values range from −0.04 to 0.02 a.u., reflecting interaction types: blue indicates strong attraction, red signifies nonbonded overlap, and green represents Van der Waals interactions. Reprinted with permission from Ref. [171]. Copyright (2018) Wiley-VCH Verlag GmbH & Co. KGaA.

durability, and excellent electrical conductivity. Diamond nanopillars were fabricated using an Au-mask-assisted reactive ion etching technique. Raman and XPS analyses confirmed the presence of sp^2-bonded carbon among sp^3-bonded carbon. While sp^2 carbon contributes to enhanced electrochemical activity, sp^3 carbon ensures increased stability during SC testing [174]. In a separate study by Zhang and co-workers developed a nanocomposite of rGO-boron carbon nitride (BCN) for high-performance fabric-based SCs. The combined effect of nanocomposite hampers the restacking of rGO sheets, which ultimately offer high surface area and electrolyte ion pathways. The rGO-BCN fiber membrane with high flexibility was developed to construct

solid-state flexible SCs. The SCs device achieved a high energy density of 31.03 W h kg^{-1} and 87.72% cycling stability after 10000 cycles [175]. Dey et al. [176] reported the synthesis of Laser-irradiated B-doped graphene and constructed a symmetric SC cell using water-in-bisalt (WIBS) electrolyte (12 mol L^{-1} $NaNO_3$ + 0.1 mol L^{-1} KNO_3). The XPS analysis showed 4.01% of B content in the graphene framework, and the symmetric SC cell achieved a high specific capacitance of 102.45 mF cm^{-2} at 0.4 mA cm^{-2} and decent cycling performance over 8000 cycles, maintaining 100% Coulombic efficiency.

Boron-doped carbon materials enhance SCs performance by improving conductivity, increasing specific surface area, and introducing active sites for enhanced pseudocapacitive behavior. However, there are challenges, including complications in synthesis methods, achieving uniform boron incorporation, and controlling its doping level to balance conductivity and capacitive properties. Cost-effective, scalable production and stability under long-term cycling in various electrolytes remain critical hurdles.

3.1.4. Oxygen-doped carbon for supercapacitors

In energy storage and conversion research, the influence of oxygen doping is still not fully understood, with few studies examining its underlying mechanisms. Despite often being overlooked, oxygen atoms play a crucial role in energy storage, particularly with acidic electrolyte-based SCs and batteries [177]. Different oxygen species can be introduced into carbon electrodes depending on precursor type, treatment, and activation processes. Although many materials naturally contain oxygen, its effect on material properties is rarely explained.

According to the literature, the XPS spectrum of oxygen (O 1s) can be separated into three distinct peaks associated with C–O, O–H, and C═O bonds, found at 531.1 (± 0.2), 532.4 (± 0.3), and 533.8 (± 0.3) eV, respectively [178]. Functional groups containing oxygen, which can also incorporate additional heteroatoms or related groups, are commonly present on the carbon surface. These groups significantly impact capacitive performance by participating in faradaic reactions, which enhance the specific capacitance of carbon materials in aqueous SC systems.

Carbon materials contain a range of oxygen-based functional groups that can be grouped based on their interactions with water: acidic types (e.g., carboxyl and anhydride), neutral or weakly acidic types (such as phenolic, epoxy, and ether groups), and basic types (like quinone and carbonyl) (Fig. 8). The properties of these groups are influenced by their atomic hybridization, with sp^2-hybridized oxygen atoms acting as electron acceptors, while sp^3-hybridized oxygen atoms tend to donate electrons. These functional groups are distributed differently within the graphite structure: double-bonded groups such as carboxyl and carbonyl often appear at sheet edges. In contrast, hydroxyl and epoxy groups are more evenly spread. Double-bonded groups like carboxyl and carbonyl disrupt the extended conjugation within graphite's hexagonal ring system, requiring higher energy for their formation. Consequently, unlike single-bonded carbon-oxygen groups, they preferentially localize at the more reactive sheet edges. The surface characteristics of carbon have a major effect on the adsorption process. Hydroxyl and quinone groups are the primary contributors to improved capacitance among oxygen-containing groups. However, these groups also increase the

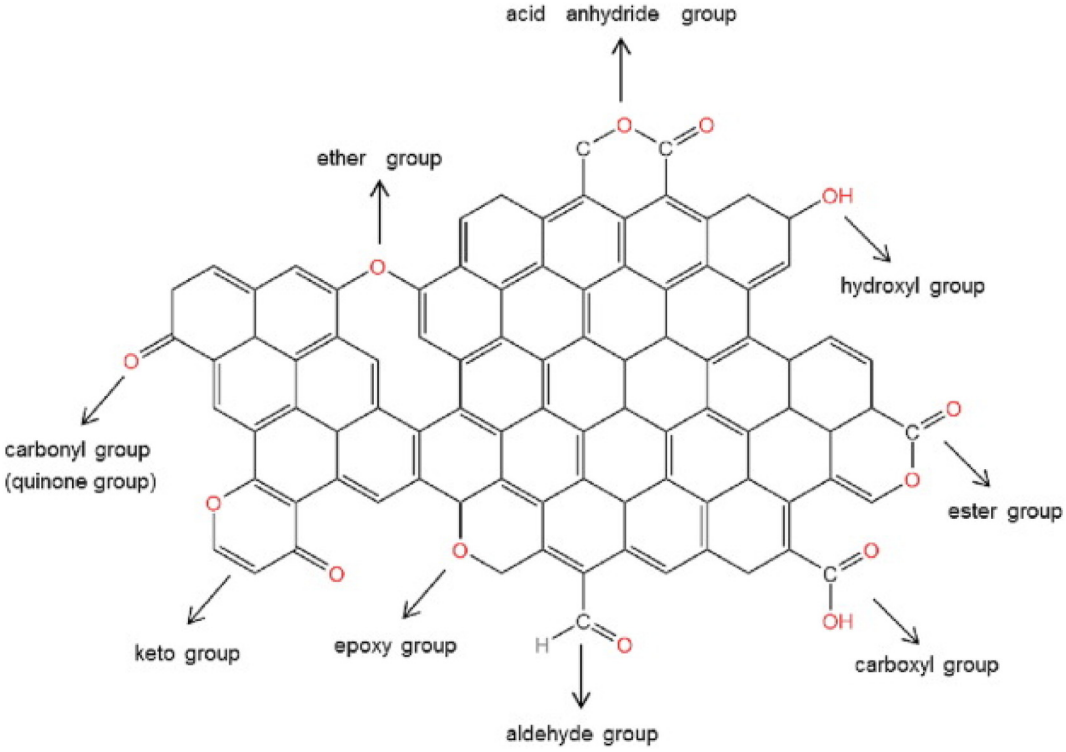

Fig. 8. Typical oxygen species and oxygen-functional groups in carbon. Reprinted with permission from Ref. [179] Copyright (2023) Elsevier.

internal resistance of electrodes, inhibiting electric double-layer formation. In addition, the quasi-reversible redox reactions associated with these groups can degrade cycling performance. Therefore, it is crucial to carefully design both the types and amounts of oxidizing functional groups [179].

It was confirmed that O–H groups enable the adsorption of Na^+ ions, while C═O groups participate in a surface–redox reaction with Na^+ ions as,

$$C=O+Na^{+}+e^{-}\leftrightarrow -C-O-Na \quad (4)$$

Furthermore, the dopant is an attractant for the OH group, making the material more prone to oxidation and altering its affinity for Na. This susceptibility can sometimes lead to irreversible changes in battery performance due to the formation of hydroxide or water. Calculations indicate that when a doped graphene-based material is used as the sodium battery electrode, the dopant type determines the optimal oxidation level, thus impacting the material's Na ion storage performance [180].

3.1.5. Fluorine-doped carbon for supercapacitors

Fluorine doping, or fluorinating carbon materials, involves attaching fluorine atoms directly to the carbon surface rather than incorporating them into the carbon lattice [181]. In some 2D carbon structures, fluorine atoms inserted between layers increase the spacing, which helps in fast charge storage. Among non-metal dopants, fluorine stands out with a high electronegativity of 4.0, surpassing elements like chlorine (3.0), bromine (2.8), and commonly used dopants such as nitrogen (3.0), sulfur (2.5), and boron (2.0). This results in a highly polarized C–F bond, concentrating electron density on the fluorine atom, a property that enhances the effectiveness of fluorinated carbon materials as electrodes in SCs. The addition of fluorine atoms boosts the charge storage ability of carbon materials [182].

The charge storage mechanism in fluorinated carbon materials for electrochemical capacitors mainly relies on EDLC-type storage, which involves the reversible adsorption and desorption of ions, such as H_3O^+ ions, in the H_2SO_4 electrolyte. Studies, including computer simulations and experimental observations, show that in both aqueous and organic electrolytes, the highly electronegative surface of fluorinated carbon materials strengthens the interaction between electrolyte ions and the carbon surface, resulting in enhanced EDLC performance. The semi-ionic C–F bond, which is intermediate between ionic and covalent bonds, is recognized as a critical factor contributing to improved charge storage in fluorinated carbon materials for SCs. The C–F bond can vary; the ionic bond type shows weaker interaction, leaving the carbon atoms close to an sp^2 configuration, while covalent C–F bonds are more stable [181]. Fluorine-doped materials often exhibit an acidic nature and act as electron acceptors. This property contributes to fluorinated carbon materials stability and improved electron transfer capabilities with semi-ionic C–F bonds. Additionally, fluorine incorporation can lead to structural modifications in carbon materials, such as creating surface wrinkles and pores. These features increase the specific surface area, enabling more excellent charge storage and higher specific capacitance in SCs.

In recent studies, fluorine-rich nanoporous carbons with tunable porosity were synthesized using a silane precursor. The polar fluorinated surface enhances wettability with organic electrolytes, achieving a specific capacitance of 168 F g^{-1} and excellent stability. The authors theoretically demonstrated that incorporating fluorine atoms into carbon clusters increases the electronegativity of the surrounding regions, thereby modifying their interactions with electrolyte ions (Fig. 9a and b). Fang and coworkers recently developed fluorine-doped graphene sheets via electrochemical exfoliation, which were used as electrodes in flexible wearable supercapacitors (FSCs). These F-doped graphene nanosheets possess atomic-level thickness, uniform lateral sizes of 1–5 μm, and a fluorine doping concentration of 3.5 at%, making them ideal for scalable production of flexible SCs (Fig. 9c). The ionogel-based FSCs achieve a high operating voltage of 3.0 V, delivering an impressive areal energy density of 213.4 μWh cm^{-2} at a power density of 1.45 mW cm^{-2}. Furthermore, the F-doped FSCs demonstrate exceptional mechanical flexibility, retaining full capacitance even when bent at 180°, and exhibit strong thermal stability up to 80 °C (Fig. 9d and e) [184]. Zhou and co-workers [185] developed fluorine-modified graphene nanosheets for ionogel-based micro-SCs. Using electrochemical exfoliation, they simultaneously achieved intercalation and fluorination of graphene nanosheets with fluorine-containing inorganic salts under mild, neutral conditions. The resulting FG nanosheets exhibit an atomically thin structure, large lateral dimensions of up to 12 μm, a high yield of over 70% with no more than 3 layers, and uniform fluorine incorporation at 3 at%. The ionogel-based micro-SCs delivered an energy density of 56 mWh cm^{-3}. The authors have shown that the fluorine incorporation creates numerous electrochemically active sites, i.e., C–F bonds, which thus provide additional pseudocapacitance. In another study by Lu and coworkers, F-doped graphene aerogels were prepared by hydrothermal. The semi-ionic C–F bonds formed during fluorination offered high conductivity and enhanced electrochemical performance. The symmetric SCs with a present material offered an energy density of 26.2 W h kg^{-1} at a power density of 899 W kg^{-1} [186]. Previous studies indicated that biomass-derived ACs suffer from poor rate performance due to long ion diffusion pathways and low mesopore volume. To address this, Kim et al. [182] developed fluorine-doped mesoporous ACs while conducting fluorine impregnation and KOH activation simultaneously during carbonization. This approach significantly increased the specific surface area to 2710 m^2 g^{-1}, much higher than undoped ACs. The resulting material also achieved a high specific capacitance of 184 F g^{-1} and excellent rate capability, demonstrating that fluorine doping enhances SCs performance. The improved electrochemical properties are largely due to the synergistic effect between F atoms and other heteroatoms. However, the impact and mechanism of F atom doping on the electrochemical behavior of carbon atoms remain unclear.

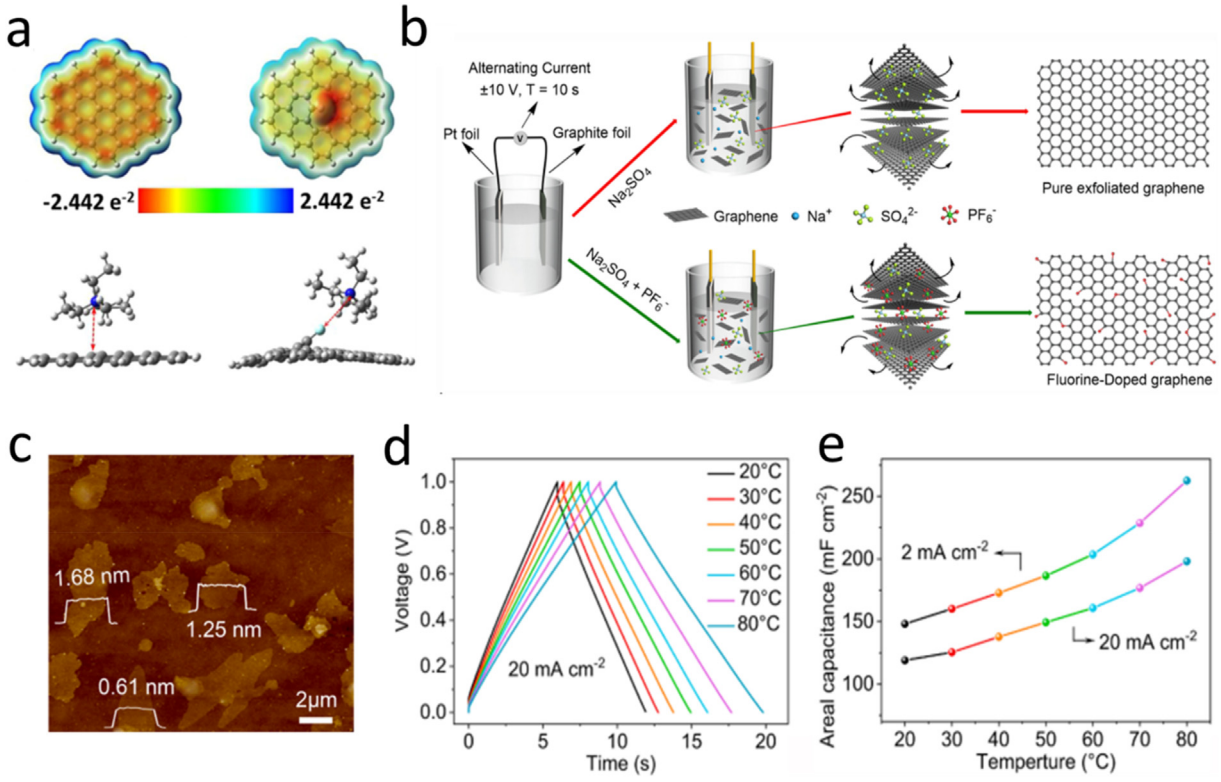

Fig. 9. (a) Simulated electrostatic potential surface for pristine graphene and F-doped graphene. Reprinted with permission from Ref. [183]. Copyright (2016) Elsevier. (b) Synthesis protocol for F-doped graphene nanosheets, (c) AFM depiction for F-doped graphene nanosheets, and (e) GCD profiles of F-doped graphene at different current densities across different temperatures and corresponding areal capacitance. Reprinted with permission from Ref. [184]. Copyright (2024) Elsevier.

3.1.6. Phosphorus-doped carbon for supercapacitors

Phosphorus (P)-doped carbon materials are gaining attention as effective electrode materials for SCs, thanks to their improved electrochemical performance [187]. Incorporating P into carbon matrices improves the material's conductivity and introduces beneficial pseudocapacitance, contributing to increased energy and power densities of SCs. This doping process optimizes the material's electrical properties and influences its surface chemistry and electrochemical stability. As a result, P-doped carbon materials have garnered significant attention for their potential to advance SC technology, offering improved performance and greater efficiency in energy storage applications. P-doped three-dimensional hierarchical porous carbons (P-3DHPCs) were recently synthesized using a direct pyrolysis approach (Fig. 10a). The phosphorus species were introduced into carbon during carbonization, which caused pore structure development. SCs performance tested in 6 mol L^{-1} KOH electrolyte show a high specific capacitance of 367 F g^{-1} at 0.3 A g^{-1} and a long cycling stability (96.5% after 10,000 cycles at 3 A g^{-1}) [188]. Monte and coworkers [189] developed a P-doped carbon-CNT composite to attain good SCs performance. SEM image (Fig. 10b) demonstrated the development of a fibrillar network composed of multi-walled carbon nanotubes (MWCNTs) encased in carbon colloids. The electrochemical performance of the obtained material was tested in a 2 mol L^{-1} H_2SO_4 electrolyte. The electrode shows pseudocapacitive behavior, which was assigned to the effect of phosphate moieties. P-doped carbon–CNT composites presented a specific capacitance of 220 F g^{-1} with energy densities of 22.6 W h kg^{-1} at a power density of 10 kW kg^{-1}. A carbon wood (CW) with a high phosphorus content (9.24 at%) is obtained by phytic acid treatment on porous wood [190]. Phytic acid's six negatively charged phosphate groups deliver numerous cross-linking sites, allowing for significant phosphorus doping on carbon. The symmetric SCs (SCs) made with P-3DHPCs showed a specific capacitance of 206.5 F g^{-1} at 1.0 mA cm^{-2}, 90.5% stability after 20,000 cycles, and a high energy density of 41.2 Wh kg^{-1} at a power density of 26.3 W kg^{-1}. DFT analysis was used to investigate the effects of phosphorus doping on edge-passivated carbon. This analysis showed that the doped phosphorus atoms function as positive charge centers, whereas adjacent carbon and oxygen atoms, owing to their greater electronegativity, exhibit characteristics of negative charge centers (Fig. 10c). PDOS analysis shows that P and O atoms, especially P2, and P5, and select O atoms, have significant electron distribution near the Fermi level, enhancing electron exchange in reactions compared to carbon (Fig. 10d). Frontier orbital analysis confirms that HOMO and LUMO are mainly localized around doped and adjacent atoms. Phosphorus

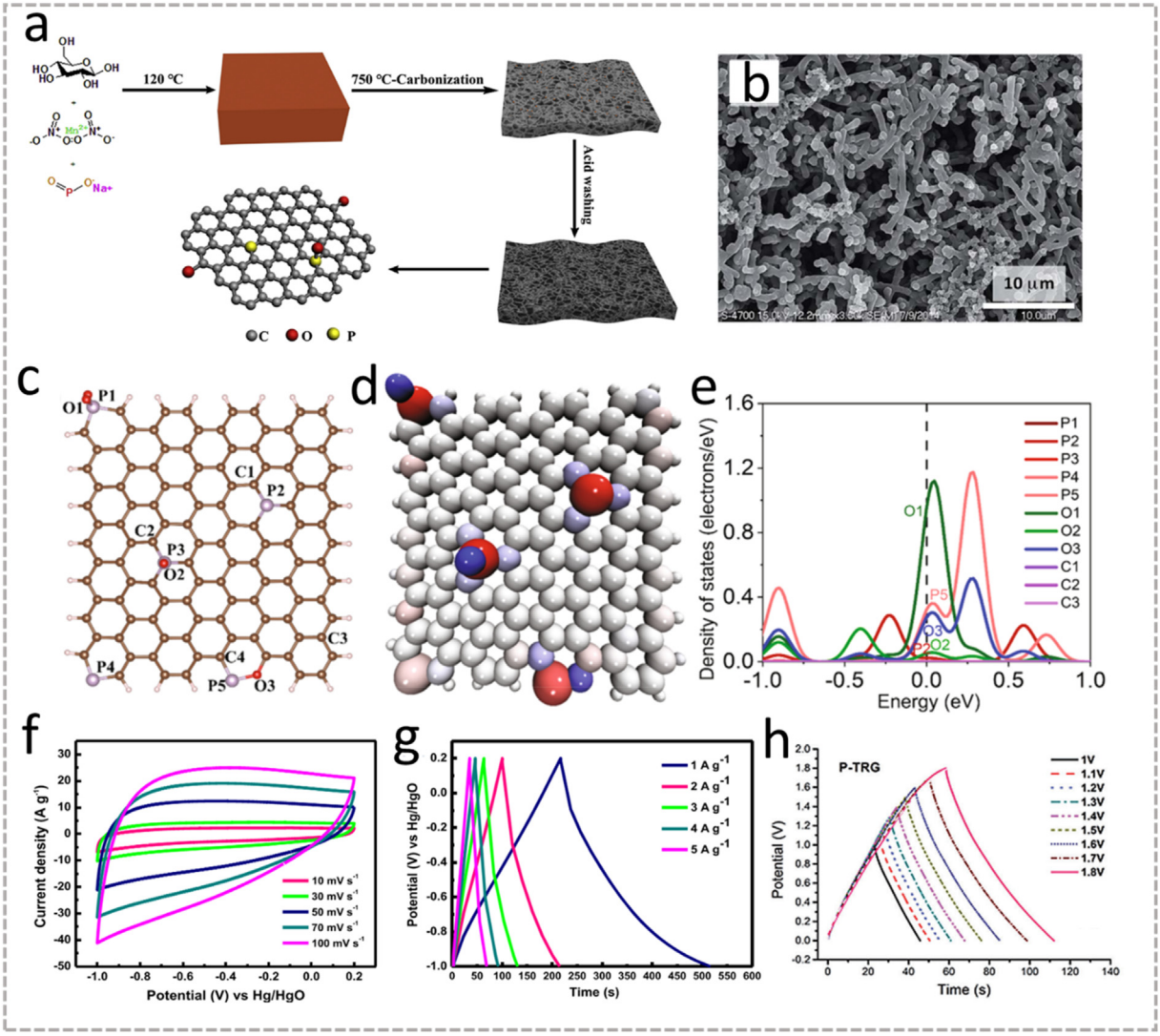

Fig. 10. (a) Synthesis protocol for the fabrication process of P-3DHPCs. Reprinted with permission from Ref. [188]. Copyright (2018) Elsevier. (b) SEM image of P-doped carbon-CNT composite. Reprinted with permission from Ref. [189]. Copyright (2016) The Royal Society of Chemistry. (c) The optimized carbon layer doped with P and O, with edge carbon atoms passivated by hydrogen. (d) Bader charge analysis: positive charges in red, negative in blue, with darker shades indicating greater intensity. (e) PDOS of p orbitals of P and O atoms and s orbitals of C atoms from structure (c). Reprinted with permission from Ref. [190]. Copyright (2021) Elsevier. (f) CV and (g) GCD curves for P-doped porous carbon. Reprinted with permission from Ref. [192]. Copyright (2021) Elsevier. (h) GCD of P-TRG at different potential windows. Reprinted with permission from Ref. [193] Copyright (2015) Wiley-VCH Verlag GmbH & Co. KGaA.

doping enhances electrode material polarity and activity, explaining high capacity in highly phosphorus-doped wood-derived carbon (Fig. 10e).

Moreover, Lin and coworkers prepared P-doped carbon from sawdust and phosphoric acid via a one-step carbonization procedure [191]. The P-doped carbon materials developed in this study feature a high surface area, a well-defined pore size distribution, and consistent phosphorus doping, leading to outstanding electrochemical performance. Specifically, the PC-900 sample demonstrated a notable specific capacitance of 292 F g^{-1} at a current density of 0.1 A g^{-1}, and it maintained 98.3% of its initial performance after 5000 cycles in a 1 mol L^{-1} H_2SO_4 electrolyte. Additionally, the SCs device reached an energy density of 10.6 Wh kg^{-1} at a power density of 224.8 W kg^{-1} with a discharge current of 0.5 A g^{-1}. In another work, Ariharan and coworkers [192] reported self-phosphorus-doped porous carbon (P-PC) from honey wine pod fluff by direct carbonization without using the activation method. The P-PC had a surface area of 756 m^2 g^{-1}. Fig. 10f and g illustrate the CV and GCD of the P-PC. The CV curves displayed an almost rectangular outline with minor redox peaks, demonstrating a mix of EDLC and pseudo-capacitive behavior. This pseudo-capacitance ascends from the carbon surface's heteroatoms (P and O). The P-PC electrode achieved a specific capacitance of 253 F g^{-1} at 1 A g^{-1}, demonstrating good rate performance and cycling stability.

Phosphorus doping boosts the pseudocapacitance and broadens the potential window of carbon materials used as electrodes in SCs, improving energy and power density. Jurcakova et al. [193] synthesized phosphorus-doped graphene

with a phosphorus content of 1.30 atomic percent by annealing graphene with phosphoric acid. This P-doped graphene was evaluated as a supercapacitor electrode in a 1 mol L^{-1} H_2SO_4 electrolyte. The doped material demonstrated a remarkable improvement in specific capacitance and cycling stability compared to its undoped counterpart. Specifically, the phosphorus-doped thermally reduced graphene (P-TRG) achieved a capacitance of 115 F g^{-1} at a current density of 0.05 A g^{-1}, significantly outperforming the undoped TRG-800, which exhibited a capacitance of only 29 F g^{-1} under the same conditions. Furthermore, the P-doped graphene electrode operated effectively across a broad voltage window of 1.7 V (Fig. 10h), achieving an energy density of 11.64 Wh kg^{-1} and a power density of 831 W kg^{-1}, the material exhibits minimal performance degradation (only 3%) after 5000 cycles at 5 A g^{-1}, even surpassing the water decomposition potential of 1.23 V. Table 1 shows recent advancements in heteroatom-doped carbon materials and their electrochemical performance.

Thus, the overall results indicate that heteroatom-doped carbon materials have emerged as highly promising candidates for high-performance SCs owing to their superior electrochemical characteristics. Incorporating heteroatoms introduces defects and generates abundant active sites, enhancing conductivity, ion transport, and surface wettability. These modifications boost electrochemical performance, including higher specific capacitance and improved energy density. The versatility in tailoring these properties by adjusting the type and concentration of dopants allows for their optimization across diverse energy storage applications.

3.2. Multiple heteroatom co-doped carbon materials

Co-doping offers a distinct advantage over single heteroatom doping in applications such as energy storage, conversion, and electrocatalysis, which often focus on enhancing just one specific property [126,194]. The combined doping of multiple heteroatoms can boost the overall performance of materials through synergistic interactions. As a result, recent studies have increasingly explored the benefits of dual or multi-heteroatom doping. However, precisely managing heteroatom incorporation is essential for optimizing surface characteristics and electronic properties. Introducing multiple heteroatoms increases chemical complexity, making controlled doping more challenging. Techniques commonly employed for synthesizing dual-doped carbon materials include hydrothermal methods, post-treatment doping, pyrolysis, and chemical vapor deposition (CVD), which are also utilized for single-atom doping approaches [195].

Table 1
Recent advancements in heteroatom-doped carbon materials and their electrochemical performance.

Materials	Doping element	Specific capacitance	Cycle stability	Ref.
N-doped graphene	6.62% Nitrogen	197 F g^{-1} at 0.5 A g^{-1}	98% over 5000 cycles	[208]
N-doped graphene	2.95% Nitrogen	205.3 F g^{-1} at 1 A g^{-1}	92.5% over 3500 cycles	[209]
N-doped graphene	7.2% Nitrogen	144.6 F g^{-1} at 0.2 A g^{-1}	90% over 500 cycles	[210]
N-doped porous carbon	5.43% Nitrogen	281 F g^{-1} at 0.05 A g^{-1}	95.5% over 5000 cycles	[211]
N-doped porous carbon spheres	6.5% Nitrogen	107 F g^{-1} at 1 A g^{-1}	800% over 5000 cycles	[212]
N-doped porous carbon/CNT	4.1% Nitrogen	324 F g^{-1} at 0.5 A g^{-1}	93.5% over 1000 cycles	[213]
N-doped porous carbon	3.73% Nitrogen	263 F g^{-1} at 1 A g^{-1}	96% over 10000 cycles	[214]
P-doped mesoporous carbon	-	312 F g^{-1} at 0.5 A g^{-1}	97.5% over 5000 cycles	[215]
P-doped porous carbon	-	292 F g^{-1} at 0.1 A g^{-1}	98.3% over 5000 cycles	[191]
P-doped porous carbon aerogels	2.02% Phosphorus	348.8 F g^{-1} at 5 mV s^{-1}	100% over 10000 cycles	[216]
P-doped graphene nanosheets	0.68% Phosphorus	290 F g^{-1} at 0.5 A g^{-1}	–	[217]
P-doped graphene	0.94% Phosphorus	388.5 F g^{-1} at 1 mA cm^{-2}	99% over 10000 cycles	[218]
S-doped graphene	3.47% Sulfur	320 F g^{-1} at 3 A g^{-1}	86% over 10000 cycles	[219]
S Doped graphene	2 wt% Sulfur	261 F g^{-1} at 1 A g^{-1}	90% over 10000 cycles	[220]
S-doped porous carbon	5.2 wt% Sulfur	320 F g^{-1} at 0.2 A g^{-1}	99% over 10000 cycles	[221]
B-doped porous carbon	–	285.6 F g^{-1} at 1 A g^{-1}	98% over 5000 cycles	[222]
B-doped porous carbon	3.9% Boron	379.9 F g^{-1} at 1 A g^{-1}	96.3% over 10000 cycles	[166]
B-doped graphene	2.56% Boron	113 F g^{-1} at 1 A g^{-1}	-	[223]
B-doped mesoporous graphene	12.9% Boron	336 F g^{-1} at 0.1 A g^{-1}	93% over 5000 cycles	[224]
N, P co-doped mesoporous carbon		210 F g^{-1} at 1.0 A g^{-1}	90% over 3000 cycles	[225]
N, P co-doped mesoporous carbon		210 F g^{-1} at 1.0 A g^{-1}	90% over 3000 cycles	[225]
N, S co-doped graphene aerogel	5.4% Nitrogen, 1.1% sulfur	169.4 F g^{-1} at 1.0 A g^{-1}	77.2% over 3000 cycles	[226]
S, P co-doped graphene	5.8% Sulfur, 4.8% Phosphorus	438 F g^{-1} at 10 mV s^{-1}	93.4% over 10000 cycles	[227]
N, B Co-doped porous carbon	12.1% Nitrogen, 3.74% Boron	304 F g^{-1} at 0.1 A g^{-1}	93% over 10000 cycles	[228]
N, B Co-doped porous carbon	6.63% Nitrogen, 7.27% Boron	341.5 F g^{-1} at 0.5 A g^{-1}	95% over 10000 cycles	[229]
N, B Co-doped porous carbon	9.74% Nitrogen, 12.77% Boron	188 F g^{-1} at 0.5 A g^{-1}	90% over 10000 cycles	[230]
N, B Co-doped porous carbon	7.1% Nitrogen, 8.4% Boron	268 F g^{-1} at 0.1 A g^{-1}	–	[231]
N, F Co-doped porous carbon	8.9% Nitrogen, 2.6% Fluorine	354 F g^{-1} at 0.5 A g^{-1}	–	[232]
N, F Co-doped graphene	6.21% Nitrogen, 6.98% Fluorine	366 F g^{-1} at 5 mV s^{-1}	98% over 10000 cycles	[233]
N, F Co-doped graphene	2.56% Nitrogen, 1.14% Fluorine	345.4 F g^{-1} at 1 A g^{-1}	96% over 10000 cycles	[234]
N, F Co-doped porous carbon	12.1% Nitrogen, 7.8% Fluorine	326 F g^{-1} at 1 A g^{-1}	100% over 10000 cycles	[235]

Several factors influence the SC performance. In addition to having a porous structure, heteroatom doping is an effective strategy to enhance the supercapacitive properties of carbon materials. The role of these dopants is determined by their chemical environment within the carbon framework, leading to improvements in the capacitive performance in different ways. For example, negatively charged nitrogen species can act as Faradaic reaction sites, promoting pseudo-capacitance, while quaternary nitrogen facilitates electron mobility within the carbon lattice. Additionally, introducing dopants such as sulfur, phosphorus, fluorine, and boron not only increases pseudo-capacitance and enhances electrode surface wettability but also improves the electronic conductivity of carbon by altering the electron-donor or acceptor behavior of adjacent carbon atoms [196]. Recent developments in co-doping and multi-doping approaches have shown superior capacitive performance. Carbon materials with various heteroatom dopants also exhibit unique behaviors tailored to specific applications. Generally, a higher concentration of heteroatoms results in more exposed active sites, which benefits energy storage. However, the precise location of the dopants is just as important as their concentration, with their interaction influencing overall material performance.

Theoretical calculations and experimental evidence have demonstrated that heteroatom doping alters carbon materials' electronic and chemical properties, thereby significantly enhancing their electrochemical performance, increasing interplanar spacing, and reducing structural disorder, leading to improved specific capacitance and rate capabilities [197]. By leveraging the unique benefits and synergistic effects of various heteroatoms, this approach can guide the synthesis of multiple heteroatom-doped carbon materials with superior performance.

3.2.1. N, S co-doping

N, S co-doped carbon stands out as a unique electrochemical material. Incorporating N atoms significantly enhances the conductivity of the carbon electrode, while S atoms expand the carbon layer spacing, thereby boosting charge mobility and facilitating access to active species. Consequently, this material has been widely researched and finds applications in different fields, including batteries, SCs, and electrocatalysis.

A recent investigation by Gopalsamy et al. [198] demonstrated N, S co-doped graphene nanoribbons as efficient materials for SCs. These materials were synthesized via a straightforward in-situ thermal annealing process using graphene nanoribbons along with N and S precursors. TEM images confirmed a uniform dispersion of N and S across the wrinkled graphene nanoribbons. The resulting electrode exhibited a specific capacitance of 442 F g^{-1} at 0.5 A g^{-1}, with a remarkable capacitance retention of 98.6% after 10,000 cycles in a 1 mol L^{-1} Na_2SO_4 electrolyte. Additionally, the symmetric supercapacitors achieved an energy density of 23.85 Wh kg^{-1} at a power density of 448 W kg^{-1}. These impressive results highlight the promise of dual-atom co-doping for enhanced performance. In another study, banana peel waste was carbonized and activated with KOH to produce innovative nitrogen and sulfur co-doped, hierarchically porous carbon materials (Fig. 11a). These materials exhibited a high specific surface area of 2452 m^2 g^{-1}, with nitrogen and sulfur contents of approximately 3.2 at% and 0.6 at%, respectively. When tested as electrode materials for supercapacitors, they showed a specific capacitance of 220 F g^{-1} at 0.5 A g^{-1} in a 1 mol L^{-1} Na_2SO_4 electrolyte. The CV and GCD curves for symmetric SCs cells are shown in (Fig. 11b and c). The symmetric SCs achieved a notable power density of around 2690 W kg^{-1} and an energy density of approximately 5.3 Wh kg^{-1}. This research highlights using banana peels, a promising waste resource, as a carbon precursor for synthesizing heteroatom (N, S)-doped carbons, demonstrating the potential of biomass-derived porous carbons in energy storage applications [199]. Biomass-derived carbons generally possess a hierarchical porous structure with naturally occurring N and O heteroatoms but typically have low sulfur content. To improve co-doping efficiency, a one-step carbonization method was employed using bamboo shoot shells (BSS) and PEDOT, which served as a sulfur source, to produce nitrogen and sulfur co-doped carbon (NSPC). The synthesized NSPC performed excellently, achieving a 30.60 Wh kg^{-1} at a power density of 468.75 W kg^{-1} in 1 mol L^{-1} $EMIMPF_6$ [200].

Hao and coworkers synthesized N and S co-doped 3D mesoporous carbon cubes using KIT-6 as a template and pyrrole as the precursor (Fig. 11d), achieving controlled dopant levels (nitrogen 10.0–4.6 at%, sulfur 0.94–0.75 at%). They evaluated the supercapacitive performance of the material, which demonstrated an impressive capacitance of 320 F g^{-1} at 1 A g^{-1}. This high performance was attributed to a combination of electrical double-layer capacitance and pseudo-capacitance, enhanced wettability, and improved conductivity due to the integration of N and S within the carbon framework [201]. Wang et al. synthesized N, S co-doped porous carbon nanobowls (with N and S contents of 3.3 and 1.7 wt%) using a one-pot condensation/carbonization method. These nanobowls were formed by interfacial capillary compression of carbon nanospheres, reducing voids and enhancing bulk density while preserving a microporous/mesoporous structure. The high surface area and dual N, S doping significantly boost specific capacitance and rate performance. When tested in symmetric SCs, these materials showed a volumetric capacitance of 273.4 F cm^{-3} at 0.1 A g^{-1}, energy density of 9.6 W h kg^{-1}, power density of 475.5 kW kg^{-1}, and maintained 92.4% stability after 50,000 cycles [202].

Thus, numerous studies indicate that sulfur doping complements nitrogen doping, boosting carbon materials' charge capacity and electrochemical performance. The incorporation of highly polarizable sulfur can alter the charge state of adjacent carbon atoms, thereby improving their overall capacitive performance.

3.2.2. N, P co-doping

In P-doped carbon materials, the more extended P–C bond than C–C while N-doping creates defects, leading to significant structural distortion. The low electronegativity of P

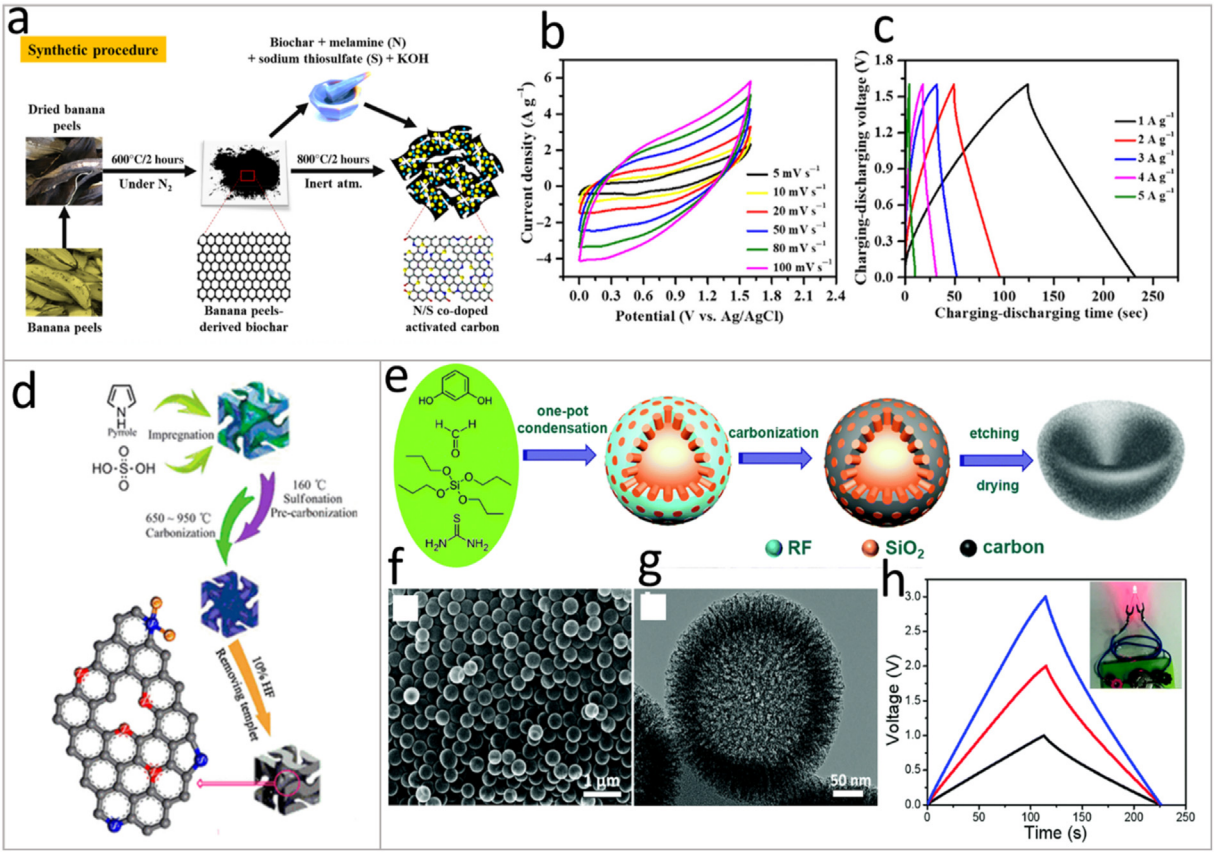

Fig. 11. (a) Synthesis protocol for the banana peels-derived biochar-based ACs with N, S co-doping, (b) and (c) CV and GCD curves of symmetric SCs cell. Reprinted with permission from Ref. [200] Copyright (2020) Elsevier. (d) A schematic illustration of the synthesis process of N, S 3D mesoporous carbon cubes. Reprinted with permission from Ref. [201]. Copyright (2014) American Chemical Society. (e) Schematic protocol for the synthesis process of carbon nanobowls. (f, g) SEM and TEM images of carbon nanobowls and (h) GCD curves for three carbon nanobowls electrode assembled SCs cell in series. Reprinted with permission from Ref. [202]. Copyright (2018) The Royal Society of Chemistry.

causes charge redistribution with C atoms. This, combined with N–P synergy, provides additional active sites and improves ion accessibility, enhancing electrochemical performance.

N, P co-doped carbon materials have attracted considerable interest in being used as SCs electrode materials. Zhang et al. [203] introduced an eco-friendly $CaCO_3$-assisted synthesis method to produce nitrogen and phosphorus co-doped hierarchical porous carbons (NPHCs) with high N (8.72 at.%) and P (4.44 at.%) content (Fig. 12a). Electrochemical testing of the materials revealed a specific capacitance of 212 F g^{-1} at 0.5 A g^{-1} and excellent retention of 75% at a high current density of 20 A g^{-1}. Additionally, symmetric SCs constructed with these materials achieved an energy density of 10.61 Wh kg^{-1} and maintained 86.3% capacitance after 10,000 cycles. This study highlights how fine-tuning chemical composition and pore architecture can significantly boost carbon electrode performance. Qiu et al. developed P, N co-doped porous carbon through direct carbonization of phosphoric acid-treated polyaniline. The resulting material features typical microporosity with a limited surface area and a narrow pore size range. The study revealed that heteroatom doping and the formation of heteroatom-containing functional groups are highly sensitive to temperature changes. The P, N co-doped microporous carbon (with doping levels of 2.7% N and 2.2% P) demonstrated superior specific capacitance, a broader operating voltage window, and improved stability compared to its non-phosphorus counterpart. Moreover, it was shown that phosphorus doping and micropore formation play a crucial role in enhancing supercapacitor performance [204]. Lin and co-workers fabricated Nitrogen and phosphorus co-doped carbon hollow spheres (NPCHSs) through carbonization and subsequent chemical activation, using dehydrated polypyrrole hollow spheres as the precursor and KOH as the activating agent. The material is heavily doped with N (11.4%), and P (3.5%). The NPCHSs form a typical 3D porous structure (Fig. 12b), resulting in a high specific surface area of 1155 m^2 g^{-1}. The CV curves at different scan rates for NPCHSs in 6 mol L^{-1} KOH electrolytes are depicted in Fig. 12c. The electrode achieved a specific capacitance of 232 F g^{-1} at a 1 A g^{-1} current density. The electrode retained 89.1% of its capacitance over 5000 cycles, making it a promising electrode material for SCs [205].

In a notable study by Bi and colleagues, nitrogen and phosphorus co-doped porous carbon (NP-HPC) was synthesized from melamine and phytic acid using in-situ K_2CO_3 activation, as illustrated in Fig. 12d. The SEM image (Fig. 12e) reveals a well-defined 3D cross-linked structure

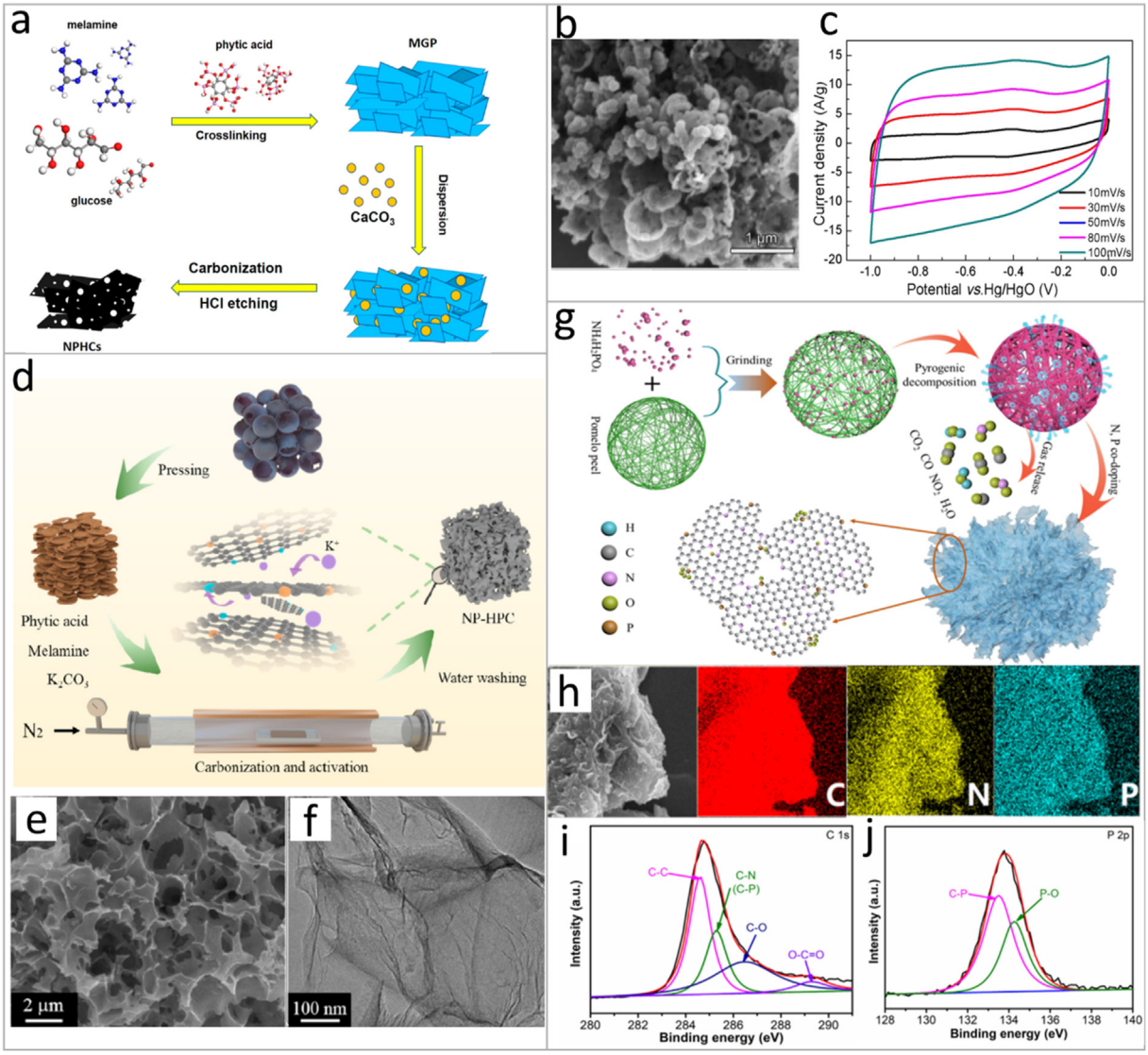

Fig. 12. (a) Synthesis protocol for the N, P co-doped carbon. Reprinted with permission from Ref. [203]. Copyright (2019) American Chemical Society. (b) SEM image for N, P co-doped NPCHSs. (c) CV curved at different scan rates for NPCHSs in 6 mol L^{-1} KOH electrolyte. Reprinted with permission from Ref. [205]. Copyright (2018) Elsevier. (d) Synthesis procedure for NP-HPC. (e,f) FESEM and TEM images for NP-HPC. Reprinted with permission from Ref. [206]. Copyright (2021) Elsevier. (g) Synthesis protocol for the N, P co-doped porous carbon nanosheets. (h) C, N, and P element mapping images. (i) C 1s and (j) P 2p XPS spectra of N, P co-doped porous carbon nanosheets. Reprinted with permission from Ref. [207] Copyright (2022) Elsevier.

with prominent macropores in the NP-HPC material. The TEM image (Fig. 12f) also shows that the 2D carbon sheets form the interconnected 3D network. This carbon framework effectively prevents the stacking of carbon layers and provides a conductive pathway, enhancing electron transport. When tested as an electrode for SCs, the NP-HPC electrode achieved a high capacitance of 358 F g^{-1} at 0.05 A g^{-1} [206]. Another exciting study by Jia and coworkers demonstrated a strategy that combines carbonization, activation, and heteroatom doping in a single step (Fig. 12g). Pomelo peel waste was utilized as the carbon precursor, and $NH_4H_2PO_4$ served as both the activator and a dual dopant for N and P atoms. The approach enabled the efficient synthesis of N, P co-doped biomass carbon nanosheets (NPCNs). The uniform distribution of N and P in carbon nanosheets was clearly visible from Fig. 12h. Furthermore, the bond structure was analyzed from the XPS studies (Fig. 12i and j). The findings suggest that the incorporation of P atoms into the carbon framework causes nearby C atoms to be pulled out of the carbon lattice plane, promoting the development of a layered structure in the biomass-derived carbon material. Moreover, symmetric SCs assembled with NPCNs offered a high energy density of 36 Wh kg^{-1} and 86% capacitance retention after 30,000 cycles [207].

Thus, the nitrogen and phosphorus co-doped carbon materials have shown great potential as electrode materials for SCs due to enhanced conductivity, surface reactivity, and improved electrochemical performance. However, challenges remain in developing efficient, sustainable methods to achieve high levels of heteroatom doping while maintaining optimal porosity. Balancing these properties is crucial for maximizing energy storage capacity and device durability.

Overall results demonstrate that heteroatom-doped carbon materials have garnered significant interest in SCs due to their enhanced electrochemical properties. The introduction of heteroatoms induces defects and creates active sites that improve conductivity, ion accessibility, and surface wettability, which, in turn, leads to enhanced electrochemical performance, such as increased specific capacitance and energy density. The ability to fine-tune these properties by varying the types and concentrations of heteroatoms makes these materials highly adaptable for a wide range of energy storage applications.

However, despite these advantages, several challenges remain. Excessive doping can destabilize the carbon framework, compromising the structural integrity and negatively impacting the long-term cycling stability of SCs. Although doping improves surface wettability and increases the number of electrochemically active sites, it can also reduce overall electrical conductivity if too many defects are introduced or if the doping levels are not optimized. Additionally, achieving uniform and controlled heteroatom incorporation often involves complex and resource-intensive synthesis processes, which can hinder scalability for industrial applications. Furthermore, while co-doping with multiple heteroatoms has shown potential synergistic effects, a complete understanding of these interactions remains elusive. The complex interplay between different dopants can sometimes yield unpredictable results, occasionally leading to performance degradation rather than enhancement. Lastly, the fundamental mechanisms of ion adsorption and charge storage in these doped systems are not yet fully understood, which makes optimizing their performance for practical applications challenging.

Addressing these challenges will require further research to balance the benefits of heteroatom doping with its potential drawbacks, alongside developing more cost-effective, scalable synthesis methods.

4. Conclusions and future perspectives

In summary, this review highlights the crucial role of heteroatom doping in enhancing the electronic properties and performance of carbon materials for SCs. Incorporating heteroatoms induces structural modifications in the carbon matrix, introducing defects and increasing active sites, enhancing electronic conductivity, ion accessibility, and surface wettability while reducing ion diffusion barriers. Additionally, certain heteroatoms can actively participate in redox reactions, further boosting supercapacitor performance. However, the research in this domain is still in its nascent stages, with several aspects yet to be fully understood. Continued investigation into single and multi-doping strategies is essential for developing next-generation SC materials. The influence of different heteroatoms varies, making direct comparisons challenging due to differences in doping levels, sites, and configurations. Although the potential synergies from multi-doping have been hypothesized, a comprehensive understanding of these interactions is still lacking.

Looking forward, several strategies can drive future advancements:

(i) Enhancing specific capacitance through increasing the content of suitable heteroatoms.
(ii) Expanding the potential window and energy density by selecting optimal heteroatoms that maintain specific capacitance while improving overall electrochemical stability.
(iii) Leveraging advanced in situ characterization techniques to gain deeper insights into structural changes, ion adsorption, and charge storage mechanisms during electrochemical processes.
(iv) Extending heteroatom-doped carbon materials beyond conventional SCs to include cost-effective metal-ion capacitors, such as sodium-ion and aluminum-ion systems, broadening their practical applications.

Despite these promising avenues, several challenges must be addressed. Excessive doping can destabilize the carbon framework, compromising structural integrity and adversely affecting the long-term cycling stability of supercapacitors. While doping improves surface wettability and the number of active sites, it may also lower overall electrical conductivity if excessive defects are introduced or if the doping concentration is suboptimal. Achieving uniform and controlled doping often requires complex and resource-intensive synthesis methods, which can impede scalability for large-scale production.

Furthermore, while multi-doping with different heteroatoms has shown potential for synergistic effects, a clear understanding of the interactions between various dopants remains elusive. The complex interplay between multiple dopants can sometimes yield unpredictable results, occasionally leading to performance degradation rather than enhancement. Moreover, the fundamental mechanisms of ion adsorption and charge storage within these doped systems are not fully elucidated, complicating the optimization of these materials for practical applications.

Ultimately, the future of heteroatom-doped carbon materials for SCs is promising due to their superior electrochemical properties and adaptability. Continued exploration of diverse doping strategies, such as incorporating nitrogen, sulfur, phosphorus, and boron, will further optimize their electronic structure and surface chemistry, enhancing energy density, power density, and cycle life. Developing scalable and cost-effective synthesis processes is crucial to translating these materials from research labs to real-world energy storage applications, potentially revolutionizing fields such as electric vehicles, portable electronics, and grid-scale energy storage.

The potential applications of these materials in SCs are vast, including electric vehicles, portable electronics, and grid energy storage systems, all of which require rapid charge and discharge cycles. Heteroatom-doped carbon materials also address limitations in conventional capacitors, contributing to more efficient, long-lasting, and environmentally friendly energy storage solutions. As research continues to explore new doping combinations and fabrication techniques, heteroatom-doped carbon materials are poised to play a pivotal role in the future of energy storage technologies.

CRediT authorship contribution statement

Pragati A. Shinde: Writing – review & editing, Writing – original draft, Formal analysis, Conceptualization. **Lok Kumar Shrestha:** Writing – review & editing, Supervision. **Katsuhiko Ariga:** Writing – review & editing, Writing – original draft, Supervision, Project administration, Funding acquisition, Conceptualization.

Declaration of competing interest

The author Katsuhiko Ariga is an Advisory Board Member for Green Energy & Environment and was not involved in the editorial review or the decision to publish this article. The other authors declare that they have no known competing financial interests or personal relationships that could have appeared to influence the work reported in this paper.

Acknowledgments

This work is supported by the Japan Society for the Promotion of Science (JSPS) KAKENHI Grant Number JP22F22368, JP20H00392, and JP23H05459.

References

[1] E. Zhang, Q. Zhu, J. Huang, J. Liu, G. Tan, C. Sun, T. Li, S. Liu, Y. Li, H. Wang, Appl. Catal. B Environ. 293 (2021) 120213.
[2] C. Song, B. Zhang, L. Hao, J. Min, N. Liu, R. Niu, J. Gong, T. Tang, Green Energy Environ. 7 (2022) 411–422.
[3] T. Kinoshita, Bull. Chem. Soc. Jpn. 5 (2022) 341–352.
[4] W. Deng, Y. Feng, J. Fu, H. Guo, Y. Guo, B. Han, Z. Jiang, L. Kong, C. Li, H. Liu, Green Energy Environ. 8 (2023) 10–114.
[5] W. Wang, Y. Xie, F. He, Y. Wang, W. Xue, Y. Li, Green Energy Environ. 8 (2023) 213–223.
[6] J. Li, Z. Zhang, W. Hu, Green Energy Environ. 7 (2022) 855–857.
[7] A. Chapman, E. Ertekin, M. Kubota, A. Nagao, K. Bertsch, A. Macadre, T. Tsuchiyama, T. Masamura, S. Takaki, R. Komoda, Bull. Chem. Soc. Jpn. 95 (2022) 73–103.
[8] Y. Fu, Y. Xu, Z. Zeng, A.-R. Ibrahim, J. Yang, S. Yang, Y. Xie, Y. Hong, Y. Su, H. Wang, Green Energy Environ. 8 (2023) 478–486.
[9] W. Raza, F. Ali, N. Raza, Y. Luo, K.-H. Kim, J. Yang, S. Kumar, A. Mehmood, E.E. Kwon, Nano Energy 52 (2018) 441–473.
[10] R.G. Shrestha, S. Maji, L.K. Shrestha, K. Ariga, Nanomaterials 10 (2020) 639.
[11] A.G. Olabi, Q. Abbas, P.A. Shinde, M.A. Abdelkareem, Energy 266 (2023) 126408.
[12] Y. Sugimoto, P. Pou, M. Abe, P. Jelinek, R. Pérez, S. Morita, O. Custance, Nature 446 (2007) 64–67.
[13] Y. Kameda, M. Kowaguchi, Y. Amo, T. Usuki, D. Okuyama, T.J. Sato, Bull. Chem. Soc. Jpn. 95 (2022) 1680–1686.
[14] K. Tada, Y. Hinuma, S. Ichikawa, S. Tanaka, Bull. Chem. Soc. Jpn. 96 (2023) 373–380.
[15] Y. Dai, H. Li, C. Wang, W. Xue, M. Zhang, D. Zhao, J. Xue, J. Li, L. Luo, C. Liu, Nat. Commun. 14 (2023) 3382.
[16] J. Pitters, J. Croshaw, R. Achal, L. Livadaru, S. Ng, R. Lupoiu, T. Chutora, T. Huff, K. Walus, R.A. Wolkow, ACS Nano 18 (2024) 6766–6816.
[17] Z. Ruan, J. Schramm, J.B. Bauer, T. Naumann, H.F. Bettinger, R. Tonner-Zech, J.M. Gottfried, J. Am. Chem. Soc. 146 (2024) 3700–3709.
[18] H. Imahori, Bull. Chem. Soc. Jpn. 96 (2023) 339–352.
[19] M. Ishii, Y. Yamashita, S. Watanabe, K. Ariga, J. Takeya, Nature 622 (2023) 285–291.
[20] Y. Hashikawa, Y. Murata, Bull. Chem. Soc. Jpn. 96 (2023) 943–967.
[21] M. Aono, K. Ariga, Adv. Mater. 28 (2016) 989–992.
[22] R.P. Feynman, California Inst. Technol. J. Eng. Sci. 4 (1960) 23–36.
[23] M. Roukes, Sci. Am. 285 (2001) 48–57.
[24] K. Ariga, K. Minami, M. Ebara, J. Nakanishi, Polym. J. 48 (2016) 371–389.
[25] K. Ariga, M. Aono, Jpn. J. Appl. Phys. 55 (2016) 1102A6.
[26] K. Eftekhari, B.V. Parakhonskiy, D. Grigoriev, A.G. Skirtach, Materials 17 (2024) 1051.
[27] S. Shoji, V. Stepanenko, F. Würthner, H. Tamiaki, Bull. Chem. Soc. Jpn. 95 (2022) 1083–1085.
[28] G. Chen, F. Sciortino, K. Takeyasu, J. Nakamura, J.P. Hill, L.K. Shrestha, K. Ariga, Chem. Asian J. 17 (2022) e202200756.
[29] K. Saito, Y. Yamamura, Bull. Chem. Soc. Jpn. 96 (2023) 607–613.
[30] T. Ohata, K. Tachimoto, K.J. Takeno, A. Nomoto, T. Watanabe, I. Hirosawa, R. Makiura, Bull. Chem. Soc. Jpn. 96 (2023) 274–282.
[31] S. Horike, Bull. Chem. Soc. Jpn. 96 (2023) 887–898.
[32] W. Wang, D. Chen, F. Li, X. Xiao, Q. Xu, Chem 10 (2024) 86–133.
[33] P.A. Shinde, Y. Seo, S. Lee, H. Kim, Q.N. Pham, Y. Won, S. Chan Jun, Chem. Eng. J. 387 (2020) 122982.
[34] J. Xiao, J. Chen, J. Liu, H. Ihara, H. Qiu, Green Energy Environ. 8 (2023) 1596–1618.
[35] X. Wang, Y. Wada, T. Shimada, A. Kosaka, K. Adachi, D. Hashizume, K. Yazawa, H. Uekusa, Y. Shoji, T. Fukushima, J. Am. Chem. Soc. 146 (2024) 1832–1838.
[36] S. Das, H. Mabuchi, T. Irie, K. Sasaki, M. Nozaki, R. Tomioka, D. Wen, Y. Zhao, T. Ben, Y. Negishi, Small 20 (2024) 2307666.
[37] G. Chen, F. Sciortino, K. Ariga, Adv. Mater. Interface 8 (2021) 2001395.
[38] Y. Yao, S. Wang, C. Wang, Z. Wu, C. Xiao, X. Guo, X. Yan, J. Qi, Y. Zhou, Z. Zhu, J. Mater. Chem. A 12 (2024) 10081–10089.
[39] D. Sharma, P. Choudhary, P. Mittal, S. Kumar, A. Gouda, V. Krishnan, ACS Catal. 14 (2024) 4211–4248.
[40] A.M. Sadanandan, J.-H. Yang, V. Devtade, G. Singh, N.P. Dharmarajan, M. Fawaz, J.M. Lee, E. Tavakkoli, C.-H. Jeon, P. Kumar, Prog. Mater. Sci. (2024) 101242.
[41] X. Guan, X. Zhang, Z. Li, S. Deshpande, M. Fawaz, N.P. Dharmarajan, C.-H. Lin, Z. Lei, L. Hu, J.-K. Huang, Chem. Mater. 36 (2024) 4511–4520.
[42] X. Yan, M. Chen, J. Wang, Z. Wang, R. Xin, D. Wu, Y. Song, S. Li, W. Zhu, C. Wang, Chem. Eng. J. 495 (2024) 153431.
[43] S. Ishihara, J. Labuta, W. Van Rossom, D. Ishikawa, K. Minami, J.P. Hill, K. Ariga, Phys. Chem. Chem. Phys. 16 (2014) 9713–9746.
[44] M. Komiyama, T. Mori, K. Ariga, Bull. Chem. Soc. Jpn. 91 (2018) 1075–1111.
[45] G. Chen, B.N. Bhadra, L. Sutrisno, L.K. Shrestha, K. Ariga, Int. J. Mol. Sci. 23 (2022) 5454.
[46] T. Tsuchiya, T. Nakayama, K. Ariga, APEX 15 (2022) 100101.
[47] C.-C. Hsu, Y.Z. Yu, C.-H. Wu, P.-Y. Lee, H.-M. Chen, S. Husain, C. Kongvarhodom, Y.-C. Hsiao, L.-Y. Lin, J. Energy Storage 80 (2024) 110316.
[48] O. Azzaroni, E. Piccinini, G. Fenoy, W. Marmisollé, K. Ariga, Nanotechnology 34 (2023) 472001.
[49] V. Milosavljevic, L. Kosaristanova, K. Dolezelikova, V. Adam, M. Pumera, Adv. Funct. Mater. 32 (2022) 2112935.
[50] A. Jancik-Prochazkova, H. Michalkova, Z. Heger, M. Pumera, ACS Nano 17 (2022) 146–156.
[51] K. Ariga, Micromachines 14 (2022) 25.
[52] K. Ariga, M. Ishii, T. Mori, Curr. Opin. Colloid Interface Sci. 44 (2019) 1–13.
[53] K. Ariga, J. Song, K. Kawakami, Phys. Chem. Chem. Phys. 26 (2024) 13532–13560.
[54] K. Ariga, Micromachines 15 (2024) 282.
[55] A. Kumar, P. Choudhary, T. Chhabra, H. Kaur, A. Kumar, M. Qamar, V. Krishnan, Mater. Chem. Front. 7 (2023) 1197–1247.
[56] M. Tipplook, H. Tanaka, T. Sudare, T. Hagio, N. Saito, K. Teshima, ACS Appl. Mater. Interfaces 16 (2024) 7038–7046.

[57] X. Lu, K. Yan, Z. Yu, J. Wang, R. Liu, R. Zhang, Y. Qiao, J. Xiong, ChemSusChem 17 (2024) e202301687.
[58] J. Jothisha, A.R. Devaraj, A. Saranya, M. Shandhiya, B. Janarthanan, M.R. Prabhu, Z.M. Riyas, S. Sharmila, Appl. Phys. A 130 (2024) 287.
[59] M. Xie, H. Lin, G. Liu, H. Yang, H. Hu, H. Dong, Y. Liu, X. Liu, Y. Xiao, J. Energy Storage 96 (2024) 112670.
[60] Y.N. Reddy, A. De, S. Paul, A.K. Pujari, J. Bhaumik, Biomacromolecules 24 (2023) 1717–1730.
[61] W. Tian, C. Wang, R. Chu, H. Ge, X. Sun, M. Li, Biomater. Res. 27 (2023) 100.
[62] Q.Y. You, M.D. Hu, H. Qian, Adv. Funct. Mater. (2024) 2315199.
[63] X. Jia, J. Chen, W. Lv, H. Li, K. Ariga, Cell Rep. Physi. Sci. 4 (2023) 101251.
[64] J. Song, W. Lyu, K. Kawakami, K. Ariga, Nanoscale 16 (2024) 13230–13246.
[65] L. Sutrisno, K. Ariga, NPG Asia Mater. 15 (2023) 21.
[66] S. Sivaselvam, E. Papasouli, J. Kunnumpurathu, C. Praveen, E.N. Koukaras, M. Rerat, P. Karamanis, R.S. Jayasree, Appl. Mater. Today 39 (2024) 102273.
[67] A.M.D.A. Junior, A.S. Ferreira, S.A. Camacho, L.G. Moreira, K.A. de Toledo, O.N.O. Jr., P.H.B. Aoki, ACS Appl. Mater. Interfaces 16 (2024) 23742–23751.
[68] M. Ravipati, S. Badhulika, Adv. Powder Technol. 34 (2023) 104087.
[69] N. Thmaini, K. Charradi, Z. Ahmed, R. Chtourou, P. Aranda, Appl. Clay Sci. 242 (2023) 107019.
[70] Q. Ye, M. Li, T. Xiao, S. Hou, Y. Deng, J. Luo, X. Tian, Int. J. Hydrogen Energy 49 (2024) 1014–1021.
[71] T. Lappi, S. Cordier, Y. Gayfulin, S. Ababou-Girard, F. Grasset, T. Uchikoshi, N.G. Naumov, A. Renaud, Sol. RRL 7 (2023) 2201037.
[72] R. Dhanabal, D. Kasinathan, A. Mahalingam, K. Madhuri, A.C. Bose, S.R. Dey, J. Mater. Sci. Mater. Electron. 34 (2023) 2205.
[73] M. Abdulrhman, S.K. Abdel-Aal, C.A. Bain, D. Raptis, F. Bernal-Texca, K.L. Wlodarczyk, D.P. Hand, J. Martorell, J. Marques-Hueso, Appl. Phys. A 130 (2024) 1–14.
[74] J. Kim, J.H. Kim, K. Ariga, Joule 1 (2017) 739–768.
[75] X. Zhang, Z. Xu, J. Xie, Y. Lu, S. Liu, X. Xu, J. Tu, B. Xu, X. Zhao, J. Energy Storage 80 (2024) 110263.
[76] L. Yu, M. Chang, M. Zhang, Y. Yang, K. Chen, T. Jiang, D. Shi, Q. Zhang, J. You, Sustain. Energy Fuels 8 (2024) 843–851.
[77] B. Zhang, X. Feng, R. Ma, R. Sheng, D. Wang, F. Chen, Y. Wang, M. Xu, L. Ai, N. Guo, Langmuir 40 (2024) 13467–13475.
[78] P.A. Shinde, S.C. Jun, ChemSusChem 13 (2020) 11–38.
[79] P.A. Shinde, A.C. Lokhande, N.R. Chodankar, A.M. Patil, J.H. Kim, C.D. Lokhande, Electrochim. Acta 224 (2017) 397–404.
[80] B. Yang, H.C. Fu, X.H. Chen, Q. Zhang, T. Li, Y.H. Luo, H.Q. Luo, N.B. Li, Appl. Surf. Sci. 630 (2023) 157460.
[81] T.A. Oyshi, M.T. Islam, J.Y. Al-Humaidi, M.M. Rahman, M.A. Hasnat, Int. J. Hydrogen Energy 64 (2024) 1011–1020.
[82] D. Gang, S. Park, J.M. Yoo, M. Gu, ACS Appl. Energy Mater. 7 (2024) 4572–4580.
[83] K. Ghosh, C. Iffelsberger, M. Konečný, J. Vyskočil, J. Michalička, M. Pumera, Adv. Energy Mater. 13 (2023) 2203476.
[84] J.-C. Feng, H. Xia, Beilstein J. Nanotechnol. 13 (2022) 1185–1200.
[85] J.-C. Feng, S.-X. Li, Z.-P. Zhang, Y. An, Q.-S. Gao, Z. Sun, H. Xia, Nano Energy 119 (2024) 109103.
[86] D. Bogachuk, J. Girard, S. Tilala, D. Martineau, S. Narbey, A. Verma, A. Hinsch, M. Kohlstädt, L. Wagner, Nanoscale 15 (2023) 3130–3134.
[87] X. Zhang, K. Matras-Postolek, P. Yang, J. Colloid Interface Sci. 636 (2023) 646–656.
[88] U.B. Nasini, V.G. Bairi, S.K. Ramasahayam, S.E. Bourdo, T. Viswanathan, A.U. Shaikh, J. Power Sources 250 (2014) 257–265.
[89] C. Zhang, N. Chen, M. Zhao, W. Zhong, W.-J. Wu, Y.-C. Jin, Int. J. Biol. Macromol. 273 (2024) 133017.
[90] W. Chaikittisilp, K. Ariga, Y. Yamauchi, J. Mater. Chem. A 1 (2013) 14–19.
[91] P.A. Shinde, N.R. Chodankar, H.-J. Kim, M.A. Abdelkareem, A.A. Ghaferi, Y.-K. Han, A.G. Olabi, K. Ariga, ACS Energy Lett. 8 (2023) 4474–4487.
[92] P.A. Shinde, A.G. Olabi, N.R. Chodankar, S.J. Patil, S.-K. Hwang, M.A. Abdelkareem, Chem. Eng. J. 454 (2023) 140246.
[93] R. Bahadur, G. Singh, Z. Li, B. Singh, R. Srivastava, Y. Sakamoto, S. Chang, R. Murugavel, A. Vinu, Carbon 216 (2024) 118568.
[94] G. Kothandam, G. Singh, X. Guan, J.M. Lee, K. Ramadass, S. Joseph, M. Benzigar, A. Karakoti, J. Yi, P. Kumar, A. Vinu, Adv. Sci. 10 (2023) 2301045.
[95] J. Huang, Y. Xie, Y. You, J. Yuan, Q. Xu, H. Xie, Y. Chen, Adv. Funct. Mater. 33 (2023) 2213095.
[96] A.G. Olabi, Q. Abbas, A.A. Makky, M.A. Abdelkareem, Energy 248 (2022) 123617.
[97] P.A. Shinde, Q. Abbas, N.R. Chodankar, K. Ariga, M.A. Abdelkareem, A.G. Olabi, J. Energy Chem. 79 (2023) 611–638.
[98] L.L. Zhang, X. Zhao, Chem. Soc. Rev. 38 (2009) 2520–2531.
[99] Y. Zhu, S. Murali, M.D. Stoller, K.J. Ganesh, W. Cai, P.J. Ferreira, A. Pirkle, R.M. Wallace, K.A. Cychosz, M. Thommes, Science 332 (2011) 1537–1541.
[100] L. Miao, Z. Song, D. Zhu, L. Li, L. Gan, M. Liu, Mater. Adv. 1 (2020) 945–966.
[101] J.H. Khan, F. Marpaung, C. Young, J. Lin, M.T. Islam, S.M. Alsheri, T. Ahamad, N. Alhokbany, K. Ariga, L.K. Shrestha, Y. Yamauchi, K.C.W. Wu, M.S.A. Hossain, J. Kim, Microporous Mesoporous Mater. 274 (2019) 251–256.
[102] H. Pan, J. Li, Y. Feng, Nanoscale Res. Lett. 5 (2010) 654–668.
[103] L.K. Shrestha, R.G. Shrestha, J.P. Hill, T. Tsuruoka, Q. Ji, T. Nishimura, K. Ariga, Langmuir 32 (2016) 12511–12519.
[104] N.R. Chodankar, H.D. Pham, A.K. Nanjundan, J.F.S. Fernando, K. Jayaramulu, D. Golberg, Y.-K. Han, D.P. Dubal, Small 16 (2020) 2002806.
[105] H.W. Park, K.C. Roh, J. Power Sources 557 (2023) 232558.
[106] A. Eftekhari, M. Mohamedi, Mater. Today Energy 6 (2017) 211–229.
[107] S. Sahoo, R. Kumar, E. Joanni, R.K. Singh, J.-J. Shim, J. Mater. Chem. A 10 (2022) 13190–13240.
[108] N.R. Chodankar, H.D. Pham, A.K. Nanjundan, J.F. Fernando, K. Jayaramulu, D. Golberg, Y.K. Han, D.P. Dubal, Small 16 (2020) 2002806.
[109] R. Chen, M. Yu, R.P. Sahu, I.K. Puri, I. Zhitomirsky, Adv. Energy Mater. 10 (2020) 1903848.
[110] H. Liu, X. Liu, S. Wang, H.-K. Liu, L. Li, Energy Storage Mater. 28 (2020) 122–145.
[111] W. Zuo, R. Li, C. Zhou, Y. Li, J. Xia, J. Liu, Adv. Sci. 4 (2017) 1600539.
[112] P.A. Shinde, S. Park, N.R. Chodankar, S. Park, Y.-K. Han, A.G. Olabi, S.C. Jun, Appl. Mater. Today 22 (2021) 100951.
[113] N. Velychkivska, A. Golunova, A. Panda, P.A. Shinde, R. Ma, K. Ariga, Y. Yamauchi, J.P. Hill, J. Labuta, L.K. Shrestha, ACS Appl. Energy Mater. 7 (2024) 2906–2917.
[114] R. Kumar, E. Joanni, S. Sahoo, J.-J. Shim, W.K. Tan, A. Matsuda, R.K. Singh, Carbon 193 (2022) 298–338.
[115] K. Ariga, Small Methods 6 (2022) 2101577.
[116] I.I.G. Inal, Z. Aktas, Appl. Surf. Sci. 514 (2020) 145895.
[117] G. Han, J. Jia, Q. Liu, G. Huang, B. Xing, C. Zhang, Y. Cao, Carbon 186 (2022) 380–390.
[118] S. Miao, K. Liang, J. Zhu, B. Yang, D. Zhao, B. Kong, Nano Today 33 (2020) 100879.
[119] Q. Jin, W. Li, K. Wang, H. Li, P. Feng, Z. Zhang, W. Wang, K. Jiang, Adv. Funct. Mater. 30 (2020) 1909907.
[120] Y. Gao, J. Zhang, X. Luo, Y. Wan, Z. Zhao, X. Han, Z. Xia, Nano Energy 72 (2020) 104666.
[121] J. Zhu, Q. Zhang, H. Chen, R. Zhang, L. Liu, J. Yu, ACS Appl. Mater. Inter. 12 (2020) 43634–43645.
[122] K. Ariga, R. Fakhrullin, Materials 16 (2023) 6367.
[123] X. Wang, C. Yang, J. Li, X.A. Chen, K. Yang, X. Yu, D. Lin, Q. Zhang, S. Wang, J. Wang, Adv. Funct. Mater. 31 (2021) 2009109.

[124] B.N. Bhadra, L.K. Shrestha, K. Ariga, CrystEngComm 24 (2022) 6804–6824.
[125] Q. Jin, K. Wang, P. Feng, Z. Zhang, S. Cheng, K. Jiang, Energy Storage Mater. 27 (2020) 43–50.
[126] X. Feng, Y. Bai, M. Liu, Y. Li, H. Yang, X. Wang, C. Wu, Energy Environ. Sci. 14 (2021) 2036–2089.
[127] D. Mohapatra, O. Muhammad, M.S. Sayed, S. Parida, J.-J. Shim, Electrochim. Acta 331 (2020) 135363.
[128] F. Liu, J. Niu, X. Chuan, Y. Zhao, J. Alloys Compd. 947 (2023) 169654.
[129] J. Peng, X. Dai, J. Huang, J. Zeng, L. Zheng, H. Chen, J. Energy Storage 59 (2023) 106498.
[130] X. Zou, C. Dong, Y. Jin, D. Wang, L. Li, S. Wu, Z. Xu, Y. Chen, Z. Li, H. Yang, Colloids Surf. A: Physicochem. Eng. Asp. 672 (2023) 131715.
[131] Q. Jiang, Y. Cai, X. Sang, Q. Zhang, J. Ma, X. Chen, Energy Fuels 38 (2024) 10542–10559.
[132] Y. Wang, H. Liu, K. Wang, S. Song, P. Tsiakaras, Appl. Catal. B Environ. 210 (2017) 57–66.
[133] M.A. Fauziyah, W. Widiyastuti, H. Setyawan, Ind. Eng. Chem. Res. 59 (2020) 21371–21382.
[134] B. Ouyang, Y. Zhang, Y. Wang, Z. Zhang, H.J. Fan, R.S. Rawat, J. Mater. Chem. A 4 (2016) 17801–17808.
[135] Y. Zou, Z. Zhang, W. Zhong, W. Yang, J. Mater. Chem. A 6 (2018) 9245–9256.
[136] J. Han, G. Xu, B. Ding, J. Pan, H. Dou, D.R. Macfarlane, J. Mater. Chem. A 2 (2014) 5352–5357.
[137] G. Chen, Z. Liu, G. Yang, Q. Zhang, T. Lan, C. Zhang, P. Li, K. Liu, S. He, Eng. Asp. 687 (2024) 133498.
[138] P.A. Shinde, N.R. Chodankar, M.A. Abdelkareem, Y.-K. Han, A.G. Olabi, Chem. Eng. J. 428 (2022) 131888.
[139] P.A. Shinde, M.F. Khan, M.A. Rehman, E. Jung, Q.N. Pham, Y. Won, S.C. Jun, CrystEngComm 22 (2020) 6360–6370.
[140] J. Dai, G. Li, Y. Hu, L. Han, J. Energy Storage 83 (2024) 110640.
[141] Y. Zheng, H. Wang, S. Sun, G. Lu, H. Liu, M. Huang, J. Shi, W. Liu, H. Li, Sustain. Energy Fuels 4 (2020) 1789–1800.
[142] L.-F. Chen, X.-D. Zhang, H.-W. Liang, M. Kong, Q.-F. Guan, P. Chen, Z.-Y. Wu, S.-H. Yu, ACS Nano 6 (2012) 7092–7102.
[143] Y. Zhao, M. Liu, X. Deng, L. Miao, P.K. Tripathi, X. Ma, D. Zhu, Z. Xu, Z. Hao, L. Gan, Electrochim. Acta 153 (2015) 448–455.
[144] T. Wang, J. Guo, Y. Guo, J. Feng, D. Wu, ACS Appl. Energy Mater. 4 (2021) 2190–2200.
[145] L.-N. Han, X. Wei, Q.-C. Zhu, S.-M. Xu, K.-X. Wang, J.-S. Chen, J. Mater. Chem. A 4 (2016) 16698–16705.
[146] B. Yan, L. Feng, J. Zheng, Q. Zhang, Y. Dong, Y. Ding, W. Yang, J. Han, S. Jiang, S. He, Appl. Sur. Sci. 608 (2023) 155144.
[147] X. Zhang, G. Han, S. Zhu, Small 20 (2024) 2305406.
[148] T.P. Mofokeng, Z.N. Tetana, K.I. Ozoemena, Carbon 169 (2020) 312–326.
[149] Y. Ding, Y. Li, Y. Dai, X. Han, B. Xing, L. Zhu, K. Qiu, S. Wang, Energy 216 (2021) 119227.
[150] X. Chen, J. Zhang, B. Zhang, S. Dong, X. Guo, X. Mu, B. Fei, Sci. Rep. 7 (2017) 7362.
[151] Z. Ji, G. Tang, L. Chen, J. Zhong, Y. Chen, G. Zhu, X. Chuan, J. Zhang, X. Shen, Chem. Eng. J. 480 (2024) 148213.
[152] S. Hajibaba, S. Gholipour, M. Pourjafarabadi, A. Bakhshayesh, M.M. Byranvand, M. Saliba, Y. Abdi, J. Energy Storage 79 (2024) 110044.
[153] Y. Fan, F. Fu, D. Yang, W. Liu, X. Qiu, J. Colloid Interface Sci. 667 (2024) 147–156.
[154] G. Ma, G. Ning, Q. Wei, Carbon 195 (2022) 328–340.
[155] C. Qiu, M. Li, D. Qiu, C. Yue, L. Xian, S. Liu, F. Wang, R. Yang, ACS Appl. Mater. Interfaces 13 (2021) 49942–49951.
[156] J.H. Kim, Y.-I. Ko, Y.A. Kim, K.S. Kim, C.-M. Yang, J. Alloys Compd. 855 (2021) 157282.
[157] S. Liu, Y. Cai, X. Zhao, Y. Liang, M. Zheng, H. Hu, H. Dong, S. Jiang, Y. Liu, Y. Xiao, J. Power Sources 360 (2017) 373–382.
[158] X. Ma, G. Ning, Y. Kan, Y. Ma, C. Qi, B. Chen, Y. Li, X. Lan, J. Gao, Electrochim. Acta 150 (2014) 108–113.
[159] W. Deng, Y. Zhang, L. Yang, Y. Tan, M. Ma, Q. Xie, RSC Adv. 5 (2015) 13046–13051.
[160] W.S.V. Lee, M. Leng, M. Li, X.L. Huang, J.M. Xue, Nano Energy 12 (2015) 250–257.
[161] Y. Xia, X. Zhao, C. Xia, Z.-Y. Wu, P. Zhu, J.Y. Kim, X. Bai, G. Gao, Y. Hu, J. Zhong, Y. Liu, H. Wang, Nat. Commun. 12 (2021) 4225.
[162] S.V. Sawant, A.W. Patwardhan, J.B. Joshi, K. Dasgupta, Chem. Eng. J. 427 (2022) 131616.
[163] J. Gebhardt, R. Koch, W. Zhao, O. Höfert, K. Gotterbarm, S. Mammadov, C. Papp, A. Görling, H.-P. Steinrück, T. Seyller, Phys. Rev. B-Condens. Mater. Mater. Phys. 87 (2013) 155437.
[164] C. Ling, F. Mizuno, Phys. Chem. Chem. Phys. 16 (2014) 10419–10424.
[165] C.N.R. Rao, K. Gopalakrishnan, A. Govindaraj, Nano Today 9 (2014) 324–343.
[166] P. Du, L. Liu, Y. Dong, W. Li, J. Li, Z. Liu, X. Wang, Electrochim. Acta 370 (2021) 137801.
[167] J. Han, L.L. Zhang, S. Lee, J. Oh, K.-S. Lee, J.R. Potts, J. Ji, X. Zhao, R.S. Ruoff, S. Park, ACS Nano 7 (2013) 19–26.
[168] S. Li, Z. Wang, H. Jiang, L. Zhang, J. Ren, M. Zheng, L. Dong, L. Sun, Chem. Commun. 52 (2016) 10988–10991.
[169] S. Umezawa, T. Douura, K. Yoshikawa, Y. Takashima, M. Yoneda, K. Gotoh, V. Stolojan, S.R.P. Silva, Y. Hayashi, D. Tanaka, Carbon 184 (2021) 418–425.
[170] D.-Y. Yeom, W. Jeon, N.D.K. Tu, S.Y. Yeo, S.-S. Lee, B.J. Sung, H. Chang, J.A. Lim, H. Kim, Sci. Rep. 5 (2015) 9817.
[171] F. Sun, Z. Qu, J. Gao, H.B. Wu, F. Liu, R. Han, L. Wang, T. Pei, G. Zhao, Y. Lu, Adv. Funct. Mater. 28 (2018) 1804190.
[172] M. Enterría, M.F.R. Pereira, J.I. Martins, J.L. Figueiredo, Carbon 95 (2015) 72–83.
[173] K.G. Govindarasu, R. Venkatesan, R.K. Rajagopal, G. Rajamanickam, P. Arumugam, J. Appl. Electrochem. 53 (2023) 1111–1124.
[174] S. Suman, D.K. Sharma, O. Szabo, B. Rakesh, M. Marton, M. Vojs, A. Vincze, S.P. Dutta, U. Balaji, D. Debasish, R. Sakthivel, K.J. Sankaran, A. Kromka, J. Mater. Chem. A 12 (2024) 21466–21467.
[175] Y. Zhang, Q. Huang, L. Zhou, H. Liu, C.-F. Wang, L. Zhu, S. Chen, Chem. Commun. 60 (2024) 5936–5939.
[176] B.B. Upreti, R.S. Dey, ACS Sustain. Chem. Eng. 12 (2024) 872–881.
[177] S. Lu, W. Yang, M. Zhou, L. Qiu, B. Tao, Q. Zhao, X. Wang, L. Zhang, Q. Xie, Y. Ruan, J. Colloid Interface Sci. 610 (2022) 1088–1099.
[178] S.J. Patil, N.R. Chodankar, S.-K. Hwang, P.A. Shinde, G.S.R. Raju, K.S. Ranjith, Y.S. Huh, Y.-K. Han, Chem. Eng. J. 429 (2022) 132379.
[179] C. Qiu, L. Jiang, Y. Gao, L. Sheng, Mater. Des. 230 (2023) 111952.
[180] A.S. Dobrota, I.A. Pašti, S.V. Mentus, B. Johansson, N.V. Skorodumova, Electrochim. Acta 250 (2017) 185–195.
[181] T. Wang, X. Zang, X. Wang, X. Gu, Q. Shao, N. Cao, Energy Storage Mater. 30 (2020) 367–384.
[182] K.-H. Kim, J.S. Lee, H.-J. Ahn, Appl. Surf. Sci. 550 (2021) 149266.
[183] H. Zhou, Y. Peng, H.B. Wu, F. Sun, H. Yu, F. Liu, Q. Xu, Y. Lu, Nano Energy 21 (2016) 80–89.
[184] K. Fang, K. Xie, G. Yan, X. Wu, Appl. Surf. Sci. 653 (2024) 159426.
[185] F. Zhou, H. Huang, C. Xiao, S. Zheng, X. Shi, J. Qin, Q. Fu, X. Bao, X. Feng, K. Müllen, Z.-S. Wu, J. Am. Chem. Soc. 140 (2018) 8198–8205.
[186] T. Jin, J. Chen, C. Wang, Y. Qian, L. Lu, J. Mater. Sci. 55 (2020) 12103–12113.
[187] M.M. Sundaram, A. Samayamanthry, J. Whale, R. Aughterson, P.A. Shinde, K. Ariga, L.K. Shrestha, Chem. Asian J. 19 (2024) e202400622.
[188] W. Yang, W. Yang, L. Kong, A. Song, X. Qin, G. Shao, Carbon 127 (2018) 557–567.
[189] J. Patiño, N. López-Salas, M.C. Gutiérrez, D. Carriazo, M.L. Ferrer, F. del Monte, J. Mater. Chem. A 4 (2016) 1251–1263.
[190] F. Wang, J.Y. Cheong, Q. He, G. Duan, S. He, L. Zhang, Y. Zhao, I.-D. Kim, S. Jiang, Chem. Eng. J. 414 (2021) 128767.
[191] G. Lin, Q. Wang, X. Yang, Z. Cai, Y. Xiong, B. Huang, RSC Adv. 10 (2020) 17768–17776.

[192] A. Ariharan, K. Ramesh, R. Vinayagamoorthi, M.S. Rani, B. Viswanathan, S. Ramaprabhu, V. Nandhakumar, J. Energy Storage 35 (2021) 102185.
[193] Y. Wen, B. Wang, C. Huang, L. Wang, D. Hulicova-Jurcakova, Chem. Eur J. 21 (2015) 80–85.
[194] P.F. Fulvio, J.S. Lee, R.T. Mayes, X. Wang, S.M. Mahurin, S. Dai, Phys. Chem. Chem. Phys. 13 (2011) 13486–13491.
[195] Y. Qiu, C. Zhang, R. Zhang, Z. Liu, H. Yang, S. Qi, Y. Hou, G. Wen, J. Liu, D. Wang, Green Energy Environ. 8 (2023) 1488–1500.
[196] Q. Du, Y. Zhao, Y. Chen, J. Liu, H. Li, G. Bai, K. Zhuo, J. Wang, Green Energy Environ. 8 (2023) 579–588.
[197] H.B. Tyagaraj, V. Mahamiya, S.J. Marje, M. Safarkhani, G. S K, E. Al-Hajri, N.R. Chodankar, Y.S. Huh, Y.-K. Han, Mater. Today Sustain. 27 (2024) 100901.
[198] K. Gopalsamy, J. Balamurugan, T.D. Thanh, N.H. Kim, J.H. Lee, Chem. Eng. J. 312 (2017) 180–190.
[199] G. Nazir, A. Rehman, S. Hussain, M. Ikram, S.-J. Park, Int. J. Energy Res. 46 (2022) 15602–15616.
[200] J. Han, Q. Li, C. Peng, N. Shu, F. Pan, J. Wang, Y. Zhu, Appl. Surf. Sci. 502 (2020) 144191.
[201] D. Zhang, L. Zheng, Y. Ma, L. Lei, Q. Li, Y. Li, H. Luo, H. Feng, Y. Hao, ACS Appl. Mater. Inter. 6 (2014) 2657–2665.
[202] J.-G. Wang, H. Liu, X. Zhang, M. Shao, B. Wei, J. Mater. Chem. A 6 (2018) 17653–17661.
[203] Y. Zhang, Q. Sun, K. Xia, B. Han, C. Zhou, Q. Gao, H. Wang, S. Pu, J. Wu, ACS Sustain. Chem. Eng. 7 (2019) 5717–5726.
[204] C. Wang, L. Sun, Y. Zhou, P. Wan, X. Zhang, J. Qiu, Carbon 59 (2013) 537–546.
[205] B. Lv, P. Li, Y. Liu, S. Lin, B. Gao, B. Lin, Appl. Surf. Sci. 437 (2018) 169–175.
[206] H. Bi, X. He, H. Zhang, H. Li, N. Xiao, J. Qiu, Renew. Energy 170 (2021) 188–196.
[207] G. Li, Y. Li, X. Chen, X. Hou, H. Lin, L. Jia, J. Colloid Interface Sci. 605 (2022) 71–81.
[208] K. Wang, L. Li, T. Zhang, Z. Liu, Energy 70 (2014) 612–617.
[209] Y.-Z. Liu, Y.-F. Li, F.-Y. Su, L.-J. Xie, Q.-Q. Kong, X.-M. Li, J.-G. Gao, C.-M. Chen, Energy Storage Mater. 2 (2016) 69–75.
[210] B. Jiang, C. Tian, L. Wang, L. Sun, C. Chen, X. Nong, Y. Qiao, H. Fu, Appl. Surf. Sci. 258 (2012) 3438–3443.
[211] B. Xu, H. Duan, M. Chu, G. Cao, Y. Yang, J. Mater. Chem. A 1 (2013) 4565–4570.
[212] Q. Abbas, P.A. Shinde, M. Mirzaeian, M. Mazur, M.A. Abdelkareem, A.G. Olabi, Electrochim. Acta 507 (2024) 145094.
[213] L. Wan, E. Shamsaei, C.D. Easton, D. Yu, Y. Liang, X. Chen, Z. Abbasi, A. Akbari, X. Zhang, H. Wang, Carbon 121 (2017) 330–336.
[214] Z. Wang, K. Wang, Y. Wang, S. Wang, Z. Chen, J. Chen, J. Fu, Nanoscale 11 (2019) 8785–8797.
[215] R. Ragavan, A. Pandurangan, G. Boopathi, I. Kim, M. Sathiskumar, S. Sagadevan, P. Sivaprakash, Inorg. Chem. Commun. 162 (2024) 112257.
[216] J. Guo, D. Wu, T. Wang, Y. Ma, Appl. Surf. Sci. 475 (2019) 56–66.
[217] V. Thirumal, A. Pandurangan, R. Jayavel, K.S. Venkatesh, N.S. Palani, R. Ragavan, R. Ilangovan, J. Mater. Sci. Mater. Electron. 26 (2015) 6319–6328.
[218] X. Fan, H. Xu, S. Zuo, Z. Liang, S. Yang, Y. Chen, Electrochim. Acta 330 (2020) 135207.
[219] N. Parveen, M.O. Ansari, S.A. Ansari, M.H. Cho, J. Mater. Chem. A 4 (2016) 233–240.
[220] S.S. Balaji, J. Anandha Raj, M. Karnan, M. Sathish, Synth. Met. 255 (2019) 116111.
[221] J. Tian, H. Zhang, Z. Liu, G. Qin, Z. Li, Int. J. Hydrogen Energy 43 (2018) 1596–1605.
[222] B.H. Poornima, T. Vijayakumar, Inorg. Chem. Commun. 145 (2022) 109953.
[223] V. Thirumal, A. Pandurangan, R. Jayavel, R. Ilangovan, Synth. Met. 220 (2016) 524–532.
[224] R. Nankya, J. Lee, D.O. Opar, H. Jung, Appl. Surf. Sci. 489 (2019) 552–559.
[225] T. Panja, D. Bhattacharjya, J.-S. Yu, J. Mater. Chem. A 3 (2015) 18001–18009.
[226] Z. Lu, X. Xu, Y. Chen, X. Wang, L. Sun, K. Zhuo, Green Energy Environ. 5 (2020) 69–75.
[227] X. Yu, Y. Kang, H.S. Park, Carbon 101 (2016) 49–56.
[228] H. Chen, Y. Xiong, T. Yu, P. Zhu, X. Yan, Z. Wang, S. Guan, Carbon 113 (2017) 266–273.
[229] J. Huang, J. Peng, J. Zeng, L. Zheng, H. Chen, J. Energy Storage 87 (2024) 111514.
[230] L. Luo, Y. Zhou, W. Yan, X. Wu, S. Wang, W. Zhao, Electrochim. Acta 360 (2020) 137010.
[231] H. Guo, Q. Gao, J. Power Sources 186 (2009) 551–556.
[232] L. Huang, Z. Luo, M. Luo, Q. Zhang, H. Zhu, K. Shi, S. Zhu, J. Energy Storage 38 (2021) 102509.
[233] P. Yan, L. Yan, J. Gao, Z. Zhang, G. Gong, M. Hou, Ionics 26 (2020) 4705–4712.
[234] Y. Chen, Y. Li, F. Yao, C. Peng, C. Cao, Y. Feng, W. Feng, Sustain. Energy Fuels 3 (2019) 2237–2245.
[235] Y. Gao, P. Cui, J. Liu, W. Sun, S. Chen, S. Chou, L.-P. Lv, Y. Wang, ACS Appl. Energy Mater. 4 (2021) 4519–4529.